The Astrophysical Journal, 770:119 (21pp), 2013 June 20 doi:10.1088/0004-637X/770/2/119

MARVELS-1: A FACE-ON DOUBLE-LINED BINARY STAR MASQUERADING AS A RESONANT PLANETARY SYSTEM AND CONSIDERATION OF RARE FALSE POSITIVES IN RADIAL VELOCITY PLANET SEARCHES

Jason T. Wright[1,2], Arpita Roy[1,2], Suvrath Mahadevan[1,2], Sharon X. Wang[1,2], Eric B. Ford[3], Matt Payne[3,4], Brian L. Lee[3,5], Ji Wang[6], Justin R. Crepp[7], B. Scott Gaudi[8], Jason Eastman[8], Joshua Pepper[9], Jian Ge[3], Scott W. Fleming[1,2], Luan Ghezzi[10,11], Jonay I. González-Hernández[12,13], Phillip Cargile[9], Keivan G. Stassun[9,14], John Wisniewski[15], Leticia Dutra-Ferreira[11,16], Gustavo F. Porto de Mello[11,16], Márcio A. G. Maia[10,11], Luiz Nicolaci da Costa[10,11], Ricardo L. C. Ogando[10,11], Basilio X. Santiago[11,17], Donald P. Schneider[1,2], and Fred R. Hearty[18]

[1] Center for Exoplanets and Habitable Worlds, 525 Davey Laboratory, The Pennsylvania State University, University Park, PA 16802, USA; jtwright@astro.psu.edu
[2] Department of Astronomy and Astrophysics, The Pennsylvania State University, 525 Davey Laboratory, University Park, PA 16802, USA
[3] Department of Astronomy, University of Florida, 211 Bryant Space Science Center, Gainesville, FL 32611-2055, USA
[4] Harvard-Smithsonian Center for Astrophysics, 60 Garden St., Cambridge, MA, USA
[5] Department of Astronomy, University of Washington, Box 351580, Seattle, WA 98195-1580, USA
[6] Department of Astronomy, Yale University, New Haven, CT 06511, USA
[7] Department of Physics, University of Notre Dame, 225 Nieuwland Science Hall, Notre Dame, IN 46556-5670, USA
[8] Department of Astronomy, The Ohio State University, 140 West 18th Avenue, Columbus, OH 43210, USA
[9] Department of Physics and Astronomy, Vanderbilt University, Nashville, TN 37235, USA
[10] Observatório Nacional, Rua General José Cristino, 77, Rio de Janeiro, RJ 20921-400, Brazil
[11] Laboratório Interinstitucional de e-Astronomia (LIneA), Rua General José Cristino 77, Rio de Janeiro, RJ 20921-400, Brazil
[12] Instituto de Astrofísica de Canarias (IAC), E-38200 La Laguna, Tenerife, Spain
[13] Departamento de Astrofísica, Universidad de La Laguna (ULL), E-38206 La Laguna, Tenerife, Spain
[14] Department of Physics, Fisk University, 1000 17th Ave. N., Nashville, TN 37208, USA
[15] HL Dodge Department of Physics and Astronomy, University of Oklahoma, 440 W Brooks St, Norman, OK 73019, USA
[16] Observatório do Valongo, Universidade Federal do Rio de Janeiro, Ladeira do Pedro Antônio, 43, CEP 20080-090, Rio de Janeiro, RJ, Brazil
[17] Instituto de Física, UFRGS, Caixa Postal 15051, Porto Alegre, RS 91501-970, Brazil
[18] Department of Astronomy, University of Virginia, 530 McCormick Road, Charlottesville, VA 22901, USA
Received 2013 January 18; accepted 2013 May 1; published 2013 June 3

ABSTRACT

We have analyzed new and previously published radial velocity (RV) observations of MARVELS-1, known to have an ostensibly substellar companion in a ∼6 day orbit. We find significant (∼100 m s^{-1}) residuals to the best-fit model for the companion, and these residuals are naïvely consistent with an interior giant planet with a $P = 1.965$ days in a nearly perfect 3:1 period commensurability ($|P_b/P_c - 3| < 10^{-4}$). We have performed several tests for the reality of such a companion, including a dynamical analysis, a search for photometric variability, and a hunt for contaminating stellar spectra. We find many reasons to be critical of a planetary interpretation, including the fact that most of the three-body dynamical solutions are unstable. We find no evidence for transits, and no evidence of stellar photometric variability. We have discovered two apparent companions to MARVELS-1 with adaptive optics imaging at Keck; both are M dwarfs, one is likely bound, and the other is likely a foreground object. We explore false-alarm scenarios inspired by various curiosities in the data. Ultimately, a line profile and bisector analysis lead us to conclude that the ∼100 m s^{-1} residuals are an artifact of spectral contamination from a stellar companion contributing ∼15%–30% of the optical light in the system. We conclude that origin of this contamination is the previously detected RV companion to MARVELS-1, which is not, as previously reported, a brown dwarf, but in fact a G dwarf in a face-on orbit.

Key words: binaries: spectroscopic – brown dwarfs – stars: individual (TYC 1240-945-1) – stars: low-mass

Online-only material: color figure

1. INTRODUCTION

The measurement of precise radial velocities (RVs) of stars has become a crucial and standard part of the exoplanetary astronomer's toolkit, and its application has now extended far beyond its early and most successful application to well-studied, single, bright, chromospherically quiet stars. A push to apply RV work to larger and thus fainter samples will result in the discovery of rare, touchstone systems that will inform planet formation.

The application to fainter stars in more crowded fields, as required, for instance, to follow up candidate transiting planets discovered photometrically, has necessitated attention to the effects of rare and unlikely blend scenarios. Since precise RVs can both suffer from and reveal the nature of these blended systems, they are complementary to photometric measurements and high spatial resolution imaging using adaptive optics (AO), and thus serve a critical role in detecting, validating, or ruling out planet candidates in a variety of situations (e.g., Konacki et al. 2003; Torres et al. 2004b; O'Donovan et al. 2007; Collier Cameron et al. 2007; Santerne et al. 2012; Borucki et al. 2013). Here, we present a case study of such an interplay in the case of an insidious signal seen in the MARVELS survey for exoplanets.

Lee et al. (2011) announced the detection of a short-period "brown dwarf desert candidate" with minimum mass $28 \pm 1.5 M_{\rm Jup}$ and period $P = 5.89$ days orbiting the F star TYC 1240-945-1 (MARVELS-1) as the first substellar companion discovered with the Sloan Digital Sky Survey-III (SDSS-III) MARVELS Planet Search (Eisenstein et al. 2011; Gunn et al. 2006; Ge et al. 2008). That work also reported analysis of

precise RVs made with the Hobby–Eberly Telescope (HET) High Resolution Spectrograph (HRS) using an iodine cell that had residuals to a one-companion fit that were surprisingly high ($\sim$100 m s^{-1}). The magnitude of these residuals was attributed to systematic errors resulting from the preliminary nature of the Doppler pipeline, which had not been optimized for work at HET.

Herein, we report followup observations with HET using a different pipeline that confirm the high residuals to a single-companion fit and reveal that they are apparently consistent with an inner companion, which we designate MARVELS-1 c^* with minimum mass of $\sim$0.8 $M_{\rm Jup}$ (where the asterisk indicates the provisional nature of the c component). MARVELS-1 c^*, if real, would be unique among the known exoplanets in the size and proximity of its larger companion. While the period of this putative inner companion is ambiguous because of aliasing issues, the most likely solution is consistent with a perfect 3:1 period commensurability ($P = 1.965$ days), indicative of a mean-motion resonance. Such a system would be superlative in many ways and present a unique puzzle and opportunity for planet formation and system evolution theorists.

We conduct an extensive examination of possible false positives of increasing unlikelihood and explore the reasons why the MARVELS survey might be especially susceptible to them. Following Sagan's maxim that extraordinary claims require extraordinary evidence, we adopt an attitude of healthy skepticism with respect to the ostensible two-companion solution. Ultimately, we find that the known $\sim$6 day companion to MARVELS-1 is, in reality, another star in a nearly face-on orbit.

1.1. Plan

In Section 2 we describe our spectroscopic and imaging data of the star MARVELS-1, including its imaged companions and the basic stellar properties of all stars in the MARVELS-1 system.

In Section 3 we describe our precise RV measurements of MARVELS-1 with data from HET and Keck Observatories, our search for periodicities, and our best double-Keplerian orbital solution.

In Section 4 we describe our photometry of the system, which shows no variability at the 0.2 mmag level at the periods of interest.

In Section 5 we describe our Markov Chain Monte Carlo (MCMC) and dynamical analysis of the system, which reveals only a few stable two-companion solutions.

In Section 6 we discuss alternative explanations for the signals we see. Sections 6.1–6.5 describe a variety of false alarm scenarios that we can rule out or seem too unlikely for further consideration. Section 6.6 describes a spectral contamination model that describes the data even better than the double-Keplerian model in Section 3. Sections 6.7 and 6.8 summarize our false alarm analysis and discusses the discovery of rare systems in large planet searches such as MARVELS.

In Section 7 we discuss how we chose the names for the objects in the MARVELS-1 system, and we summarize our findings in our concluding Section 8.

2. MARVELS-1

2.1. Basic Stellar Data

We have performed a reanalysis of the two FEROS spectra of MARVELS-1 presented by Lee et al. (2011), which have signal-to-noise ratios (S/Ns) of 340 and resolution $R \sim 48{,}000$, and also analyzed two Apache Point Observatory (APO) spectra with $R \sim 31{,}500$ and each with S/N of 210. We have extracted basic stellar parameters using three methods: Spectroscopy Made Easy (SME; Valenti & Piskunov 1996), StePar (Tabernero et al. 2012, and references therein), and an analysis by the SDSS-II Brazilian Participation Group, who used a method similar to the method of Wisniewski et al. (2012), but now including SME as implemented at Vanderbilt as a third pipeline. We obtain excellent consistency in our estimates of [Fe/H] and $T_{\rm eff}$.

Averaging the six results (spectra from two sources, each through three pipelines), we find $T_{\rm eff} = 6297 \pm 28$ K, $\log g = 4.22 \pm 0.09$, [Fe/H] $= -0.13 \pm 0.04$, and $v_{\rm mic} = 1.50 \pm 0.03$ km s^{-1}. These results have a significantly higher gravity (a difference of 2σ from Lee et al. 2011), indicating that MARVELS-1 is in fact an F9 dwarf star, not a subgiant as previously reported. Applying the formulae of Torres et al. (2010) to these new values, we find $M_* = 1.25 \pm 0.06\ M_\odot$ and $R_* = 1.48^{+0.26}_{-0.22} R_\odot$.

As we will see in later sections, there is likely $\sim$15%–30% contamination in these spectra from a cooler companion, likely a G dwarf, that may result in additional sources of systematic error in these parameters.

We have explored this possibility by analyzing the quality of the spectral synthesis fits generated with SME to extract parameters of the FEROS spectra. The χ^2 surfaces near minimum for these spectra have a parabolic character in most dimensions, indicating a well-behaved fit and a lack of multiple minima, as might be expected if contamination were a serious issue.

We quantitatively explored the effects of spectral contamination on our ability to extract precise stellar parameters by creating a synthetic test using high-S/N APO spectra of HD 172051 ($T_{\rm eff} = 5596 \pm 19$ K, $\log g = 4.56 \pm 0.24$) and HD 22484 ($T_{\rm eff} = 6063 \pm 19$ K, $\log g = 4.29 \pm 0.16$). We shifted the spectra to have the same velocity shift and scaled them so that the former (cooler) star contaminated the latter with a contribution of 30%. (We chose this level of contamination because it approximates the flux ratio expected if these particular stars were at the same distance, and is at the upper end of the contamination we expect in MARVELS-1.)

We then used the StePar code to estimate the stellar parameters of the blended spectrum and found $T_{\rm eff} = 5987 \pm 23$ K, $\log g = 4.44 \pm 0.19$. These values are, not surprisingly, intermediate to the correct values of the contributing spectra. In the case of $T_{\rm eff}$ the value from the blended spectrum is closer to the brighter star, and in the case of $\log g$ the value from the blended spectrum is consistent with that of the brighter star within the quoted uncertainties.

This test is not conclusive because the "secondary" star is more metal poor than the primary by 0.2 dex ([Fe/H] $= -0.29 \pm 0.02$ versus -0.07 ± -0.02), which may effect the final result (which yielded [Fe/H] $= -0.11 \pm 0.05$), but it does suggest that the values we derive here for MARVELS-1 are not badly affected by a contaminating spectrum. Adequate caution is therefore needed when using these parameters, which were calculated assuming an unblended spectrum.

2.2. Companions Revealed by AO Imaging

2.2.1. Data Acquisition and Reduction

We acquired images of MARVELS-1 using NIRC2 (instrument, PI: Keith Matthews) with the Keck II AO system (Wizinowich et al. 2000) on UT 2011 June 24. Our initial set

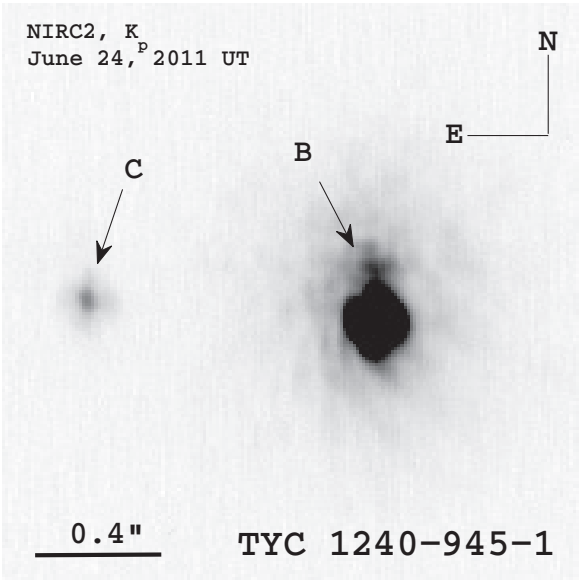

Figure 1. K' band adaptive optics image from Keck/NIRC2 showing MARVELS-1 B and MARVELS-1 C.

of observations consisted of dithered images taken with the K' ($\lambda_c = 2.12\,\mu$m) filter. Using the narrow camera setting, to provide fine spatial sampling of the NIRC2 point-spread function (PSF), we obtained nine frames with 4 s of on-source integration time each. A preliminary inspection of raw data revealed the presence of an additional point source located 0.″900 east of the primary. Upon noticing the candidate companion, we obtained images with the J-filter ($\lambda_c = 1.25\,\mu$m) to provide complementary photometry, and detected the companion at 0.″897 separation, consistent with the K' measurement.

We processed the images using standard techniques to replace hot-pixels, flat-field the array, and subtract thermal background radiation. After aligning and coadding the frames, we noticed a third object in the field, to the north of the primary star and separated by only 0.″152 in K' band (and ∼0.″18 in J band, though we adopt the K' band value because the PSF subtraction is cleaner in those images).

Figure 1 shows the image of MARVELS-1 in the K' filter. Arrows indicate the location of the 0.″9 and 0.″15 companions. Inspecting the multi-color data set, we find that neither object's position moves as a function of wavelength, demonstrating that they are not speckles. Further, the PSF of each source is qualitatively similar to that of the primary star.

In the rest of this manuscript, we will refer to the primary star as MARVELS-1 A, the 0.″9 component as MARVELS-1 C, and the 0.″15 component as MARVELS-1 B (see Section 7 for an explanation).

We performed aperture photometry to further characterize each point source using the publicly available tool Starfinder (Diolaiti et al. 2000). Often used for studying the Galactic center and other crowded fields, Starfinder is optimized for AO photometry for which numerous sources are spatially blended. By self-consistently fitting each PSF, using an empirical iterative algorithm that minimizes residuals, we were able to account for contaminating light from the much brighter primary star to measure an accurate relative brightness, angular separation, and position angle of each candidate in each filter. Our astrometric and photometric measurements for both companions relative to the primary are summarized in Table 1. MARVELS-1 C has colors comparable to an M9V dwarf ($J - K = 1.245 \pm 0.038$),

Table 1
Relative Astrometry and Photometry for the AO-resolved Components of MARVELS-1 with Respect to the A Component

Component	$\Delta K'$ (mag)	ΔJ (mag)	Separation (arcsec)	P.A. (deg)
B	2.088 ± 0.035	2.529 ± 0.056	0.153 ± 0.0017	2.6 ± 0.33
C	3.429 ± 0.021	4.311 ± 0.018	0.8998 ± 0.0003	86.25 ± 0.02

and MARVELS-1 B has colors ($J - K = 0.804 \pm 0.071$) consistent with spectral type K7V–M2V (Kraus & Hillenbrand 2007).

We have interpolated the absolute magnitude values in Table 5 of Kraus & Hillenbrand (2007) for the spectral type of MARVELS-1 A (F9V, Section 2.1) and derive M_K =3.11 and M_J =3.42. From the apparent magnitudes of MARVELS-1 ($K = 9.032 \pm 0.017$ and $J = 9.395 \pm 0.018$ according to Lee et al. 2011), we derive a rough distance of $d = 150 \pm 30$ pc from spectroscopic parallax.

MARVELS-1 C is too bright to be an M9V dwarf at the same distance as MARVELS-1 A; it is therefore likely an unbound foreground star. The colors and absolute magnitude of MARVELS-1 B are consistent with the assumption that MARVELS-1 A and B are at the same distance.

We obtain a consistent mass estimate for MARVELS-1 B of 0.62 $M_\odot$ from the relations of Delfosse et al. (2000) in both J and K band (using $M_J = 5.95$ and $M_K = 5.20$).

MARVELS-1 has a proper motion of $\dot{\alpha} = 33.6, \dot{\delta} = -5.8$ mas yr^{-1}. With more than a one year time baseline from our first epoch observations, future precision astrometric measurements using NIRC2, which has a plate scale of 9.963 ± 0.006 mas (Ghez et al. 2008), will be sufficient to determine whether the two visual companions share a physical association with the primary. The angular proximity and the consistency of the MARVELS-1 B magnitudes and colors with being a dwarf at the distance of MARVELS-1 A argue that they are likely bound. Irrespective of whether these sources represent a chance alignment along the line of sight, their flux contribution must be accounted for when analyzing precise Doppler data.

3. RV OBSERVATIONS

3.1. HET Confirmation Data

Lee et al. (2011) reported nine precise RV measurements made with the HET (Ramsey et al. 1998) HRS (Tull 1998) in late 2009 with Director's Discretionary Time as part of the RV confirmation program to the discovery of MARVELS-1 *b* made with the MARVELS instrument. These nine observations were all acquired in 2009 December with an iodine absorption cell calibrant (Butler et al. 1996) at $R \sim 60{,}000$.

These nine observations were reduced with a preliminary version of a precise Doppler pipeline (provided by Debra Fischer). This pipeline included an instrumental profile model more appropriate for the slit-fed Hamilton spectrograph at Lick Observatory and other components but was not optimized for work on HRS.

These nine points had significantly higher native precision than the SMARTS and MARVELS velocities reported by Lee et al. (2011). However, these velocity errors had to be scaled by a factor of ∼15 to match the observed ∼100 m s^{-1} scatter about the single-object Keplerian fit to the data (though with a six-component Keplerian fit to only nine measurements, the residual scatter was difficult to quantify precisely). Lee et al.

(2011) attributed these high residuals to systematic errors in their less-than-optimized Doppler pipeline.

3.2. New Data

The large residuals in the HET confirmation result did not appear completely random and exhibited significant power at 0.5 day^{-1}. This and a desire to diagnose the remaining systematic errors in the Doppler pipeline led us to request Director's Discretionary Time on HET to acquire 21 additional epochs on MARVELS-1 at higher S/Ns. These new observations were made with the same spectrograph settings as the original nine observations.

Our new observations were made in late 2010 and early 2011, sufficiently long after the original observations to provide some coverage of previously unexplored orbital phases. This system is particularly challenging to observe at HET because the companion periods are so close to integer numbers of sidereal days, and the fixed elevation of HET requires that all observations occur within ∼1 hr of two sidereal times (corresponding to the rising and setting tracks of MARVELS-1). This constraint made acquiring good phase coverage problematic and complicated our ability to rule out competing and qualitatively different orbital solutions and to determine orbital eccentricities. Nonetheless, we were able to adaptively schedule our observations in the HET queue (Shetrone et al. 2007) so as to optimally explore the 2 day period and eliminate all but one among many competing orbital solutions near 2 days.

We also obtained a template and 14 velocity measurements from Keck using the slit-fed High Resolution Echelle Spectrometer (HIRES) spectrograph in 2011 August and September. These observations were reduced using the usual methods of the California Planet Survey (Howard et al. 2010; Johnson et al. 2010; Wright et al. 2011, and references therein). Due to the higher S/N of these observations compared to the HET data, the corresponding internal errors on the RV measurements are significantly smaller.

3.3. Data Analysis: Template Analysis, Raw Reduction, and Doppler Pipelines

We performed raw reduction of the echellograms from HRS using the REDUCE package of Piskunov & Valenti (2002). This package required some modifications to the slit function description to accommodate the flat-topped nature of fiber-fed spectra.

Wang et al. (2012) describe our Doppler pipeline. In brief, the code base developed by John Asher Johnson and the California Planet Survey (e.g., Howard et al. 2009, 2011a, 2011b) was modified for the HRS at HET. This code is based on the principles of Butler et al. (1996). We have demonstrated its precision on HRS spectra with the RV standard star (σ Dra), for which we achieve an rms scatter below 3 m s^{-1} (Wang & Wright 2011; Wang et al. 2012).

Our HET observations of MARVELS-1 are not strictly analogous to our σ Dra observations, however, in that we have a lower S/N in both the template and RV observations. To put a very conservative upper limit on the systematic errors inherent in our Doppler pipeline on fainter targets, we analyzed three other MARVELS targets, TYC 1194-144-1, TYC 3413-2471-1, and TYC 3410-1406-1, in a manner identical to MARVELS-1.

We stress that these targets were observed at significantly lower S/Ns than MARVELS-1 as exploratory science and so their RVs should have considerably higher random and systematic noise. These three stars represents our entire HET sample of non-binary MARVELS targets, at present; we have no reason to consider these to be RV stable stars, since these are, to our knowledge, the first precise RV measurements ever obtained on these targets.

We present these three RV targets in Figure 2. The noisiest velocities here are for TYC 1194-144-1, with an rms dispersion of 25 m s^{-1}; the best are for TYC 3413-2471-1, at 9.5 m s^{-1}. Our MARVELS-1 observations were made at higher S/Ns and we have no reason to suspect MARVELS-1 has levels of jitter this large; we thus expect to achieve significantly better precision on MARVELS-1, closer to our performance on σ Dra.

We obtained an iodine-free stellar template at $R = 120{,}000$ for this target, but the S/N was low due to the faintness of the star and the slit losses at this high spectral resolution at HRS. We opted therefore to use the deconvolved stellar template obtained from Keck observatory. This template produced superior internal errors in the HET velocities.

All of our HET and Keck velocities appear in Tables 2 and 3. The reported uncertainties are "internal" errors measured by the consistency with which different portions of the spectrum ("chunks") report the RV of the star (Butler et al. 1996).

Table 2
HET Radial Velocities for MARVELS-1

Time BJD−2,440,000 (UTC)	Velocity (m s^{-1})	Uncertainty (m s^{-1})
15175.5879	623.88	17.6
15177.6109	1391.46	17.5
15178.5997	−979.18	16.6
15180.7994	−1038.28	17.1
15181.7885	1291.27	16.8
15182.7878	2433.65	17.4
15183.5788	1186.79	15.1
15184.5782	−1170.84	18.1
15185.5711	−2840.64	14.6
15483.7415	2159.31	13.5
15483.7528	2142.75	14.7
15484.9464	−489.47	13.5
15484.9577	−507.08	12.7
15485.7397	−2353.73	14.4
15485.7510	−2359.49	17.4
15497.7059	−2631.09	18.7
15498.7192	−2078.22	15.5
15498.9215	−1623.45	20.6
15499.7351	359.36	16.4
15500.6947	2311.46	18.1
15500.9073	2468.96	17.6
15501.6961	1699.77	18.4
15507.6863	1526.22	14.1
15510.6632	−1762.64	15.0
15510.6715	−1711.09	15.5
15522.6391	−1285.58	18.2
15522.6469	−1283.72	16.5
15522.6547	−1258.66	17.9
15522.8492	−777.53	17.7
15522.8570	−728.73	15.8
15523.6459	1120.44	13.0
15524.6390	2472.26	17.2
15524.8380	2341.07	18.8
15527.6284	−2843.01	15.2
15531.6080	708.58	17.2
15576.7008	1109.81	21.7
15577.7000	2483.02	16.9

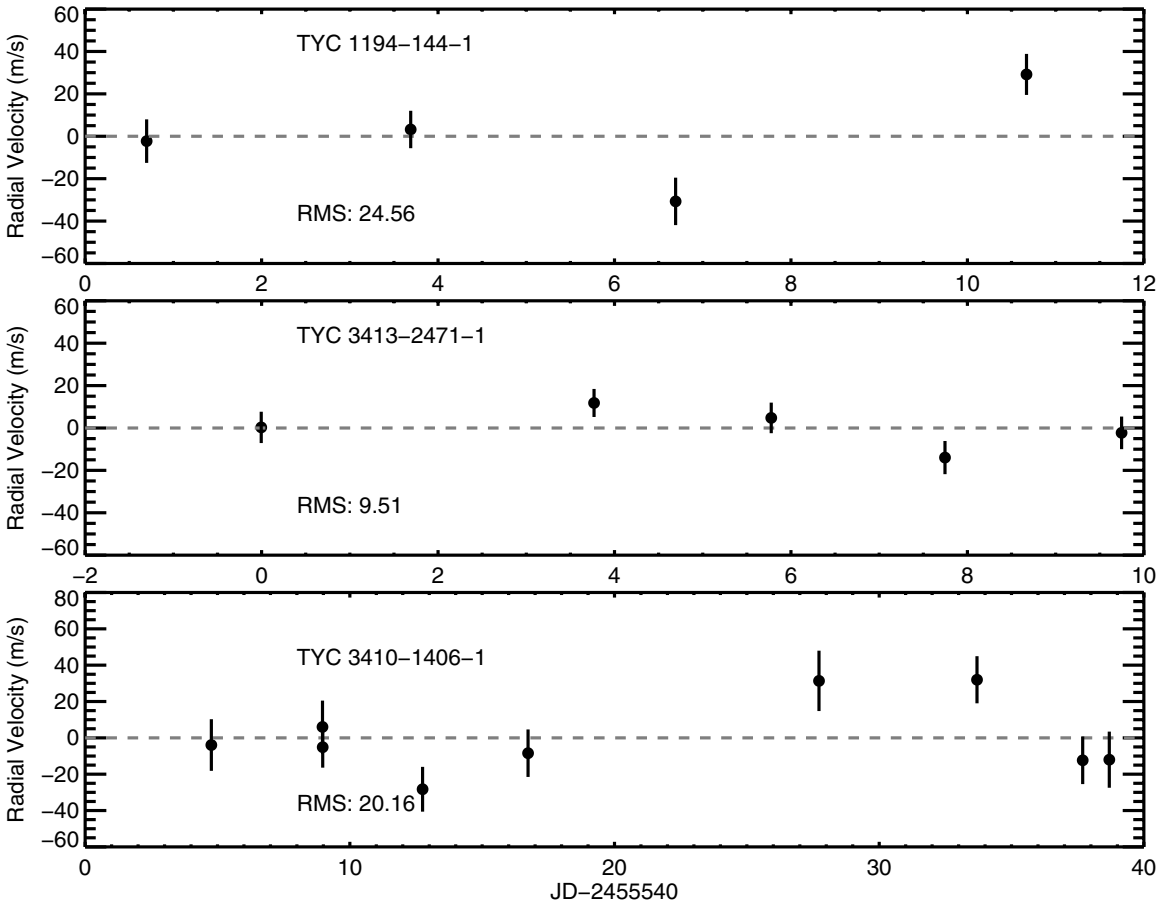

Figure 2. Radial velocities for three other MARVELS targets of similar apparent visual magnitude to MARVELS-1, but observed at lower signal-to-noise ratios and analyzed using noisier template observations. These observations represent a conservative upper limit to any systematic errors in our Doppler pipeline as applied in practice to typical MARVELS targets. We have no a priori reason to believe that these stars are inherently RV stable, and so the rms scatter of these radial velocities (listed in each pane in m s^{-1}) represents upper limits to our precision on these targets. We expect to achieve significantly better precision on MARVELS-1, closer to our performance on σ Dra, for which pipeline achieves 3 m s^{-1}.

Table 3
Keck Radial Velocities for MARVELS-1

Time BJD−2,440,000 (UTC)	Velocity (m s^{-1})	Uncertainty (m s^{-1})
15769.0930	−2349.90	5.6
15782.1024	−680.13	4.3
15783.1275	1666.41	5.2
15789.1125	1886.25	5.5
15791.1307	838.79	3.3
15793.1094	−2244.26	5.4
15796.1305	2644.81	5.9
15797.1316	599.29	2.8
15798.0922	−1702.91	5.5
15808.0954	2335.50	6.5
15809.0594	266.61	3.1
15810.0965	−2077.35	5.6
15811.0929	−1821.60	4.6
15812.1337	643.32	3.6

3.4. Keplerian Fit

We first performed a standard double-Keplerian fit, with no accounting for dynamical (Newtonian) interactions or other sources of non-Keplerian signal.

The *b* component of the MARVELS-1 system has such a large amplitude that its orbital parameters are insensitive to the fit for the c^* component and remain largely unchanged from the values in Lee et al. (2011). Fits for this system are complicated by the fixed zenith angle of the HET (see Section 3.2), which makes it difficult to acquire good phase coverage for this object, and produce significant side lobes in the periodograms of residuals to a one-companion fit, as shown in Figure 3.

The periodogram shows two dominant peaks, near 2 days (0.5 day^{-1}) and 0.66 days (1.5 day^{-1}), which have similar amplitude and each with substantial numbers of sidelobes. These two peaks are aliases of each other (their frequencies differ by exactly 1 sidereal day^{-1}). As we describe below, only the 1.965 day peak corresponds to orbital solutions with residuals near our expectations; all of the other peaks (including the 0.66 day peak) have best fits with at least 10 m s^{-1} higher levels of residual scatter. Given that the 2 day peak has a perfect period commensurability with the primary signal and the 0.66 days does not, the 2 day peak is more likely to be the "real" signal.

Regardless of its true period, the new observations appear to strongly confirm the presence of a second periodic signal of apparent semiamplitude ∼100 m s^{-1} for MARVELS-1. We have fit all velocity points using the RVLIN package of Wright & Howard (2009), checking for a suite of orbital periods near 2 days and 0.66 days to explore all of the peaks shown in Figure 3. We assumed 9 m s^{-1} of jitter, chosen because it produced a χ^2_ν near 1 (the fit details are not strongly sensitive to the amount of jitter assumed, and we performed a more robust MCMC calculation with jitter as a parameter, as well, described

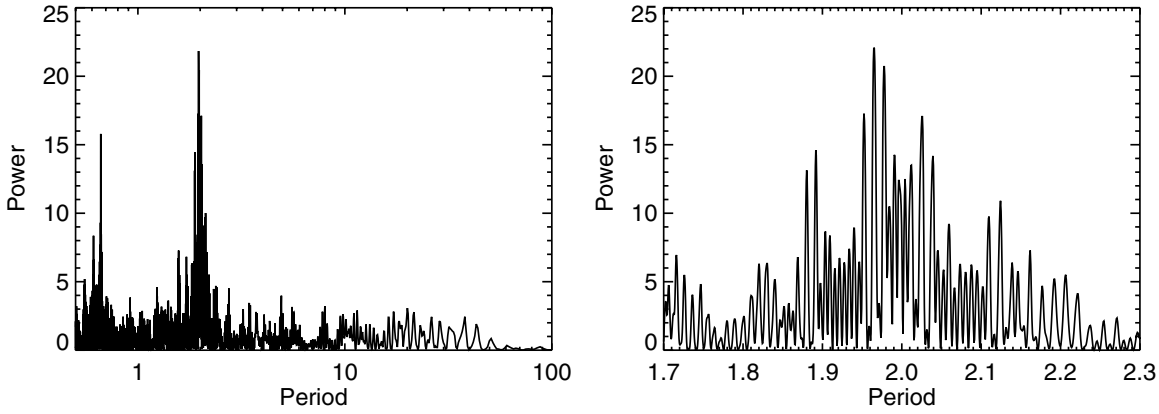

Figure 3. Left: periodogram of the residuals to a one-companion fit to the HET RV data. There is substantial power near 2 days, but severe aliasing due to the near-integer period of the c^* component produces a second peak near 0.66 days and large sidelobes to the tallest peaks. The two-companion Keplerian fit with the smallest residuals has $P_c = 1.965$ days. Right: detail near 1.965 days.

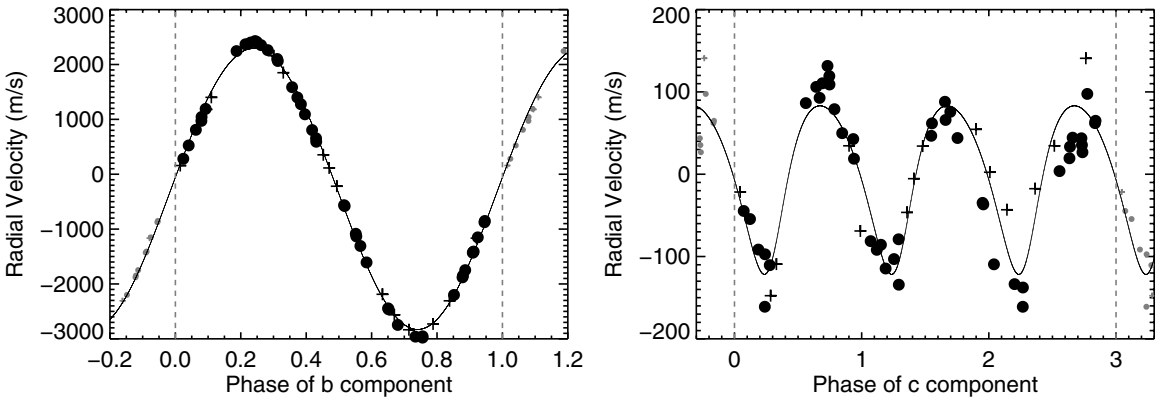

Figure 4. Solid black disks are HET velocities, crosses are Keck velocities, and small gray symbols are repeated points. Left: radial velocities phased at the period of the b component. On this scale, the effects of the c^* component are just visible. The internal (random) errors are smaller than the large plotted points. Right: residuals phased to the period of MARVELS-1 b given in Table 4, showing three consecutive periods (only the gray points are repeated). Deviations from a Keplerian curve are large and appear to be a consistent function of phase of the b component. Note also that the zero crossings occur simultaneously with the zero crossings of the b component. We phase both diagrams to have phase zero at the velocity zero with positive slope of the primary component.

Table 4
Formal Best-fit Keplerian Orbital Elements for Substellar Companions in the MARVELS-1 System

Property	b	c^*
Per (d)	5.895394(63)	1.96492(29)
T_0 (JD−2,440,000)	15498.059(91)	15498.770(91)
e	0.0160(16)	0.134(56)
ω (°)	179.7(5.5)	306(19)
K (m s^{-1})	2572.6(4.0)	104.8(4.4)
$m \sin i$ ($M_{\rm Jup}$)	27.6(1.5)	0.764(42)
a (AU)	0.0702(19)	0.03351(91)
rms (m s^{-1})	14.7	
χ^2_ν	1.01	
Jitter (m s^{-1})	9	
$N_{\rm obs}$	30	

Notes. This fit is dynamically unstable. For succinctness, we express uncertainties using parenthetical notation, where the least significant digit of the uncertainty, in parentheses, and that of the quantity are to be understood to have the same place value. Thus, "0.100(20)" indicates "0.100 ± 0.020," "1.0(2.0)" indicates "1.0 ± 2.0," and "1(20)" indicates "1 ± 20." Note that the parameters of our best model for the system appear in Table 7, not here.

in Section 5.1). The parameters of this best two-companion fit are shown in Table 4. We calculated parameter uncertainties for this fit using bootstrapping methods with the BOOTTRAN routine (Wang et al. 2012).

Figure 4 shows the measured velocities after subtracting the solution for the b component from the best two-companion fit. The temporal baseline of the velocities spans over a full year, giving coverage of most phases of the orbit at this best-fit period. The rms to the fit (the standard deviation of the residuals, with no adjustment for the number of model parameters) is 14.7 m s^{-1}.

Under the assumption that the c^* component is real, we would attribute this 9 m s^{-1} of jitter needed to achieve χ^2_ν near 1 to strong gravitational perturbations (see Section 5.3).

4. PHOTOMETRY

The transit search photometry of Lee et al. (2011) using KELT data (Pepper et al. 2007; Siverd et al. 2009) rules out photometric variability on the period of either RV signal at the submillimagnitude level; their Figure 3 illustrates that the star is photometrically constant.

We have reanalyzed these data and find that there is no evidence for periodic variability, and the limits for $P = 1$–10 days are quite stringent. The strongest peak in the periodogram in that interval has $P = 1.0218$ days with amplitude 0.87 ± 1.8 mmag, and we associate this peak with diurnal effects. At the periods of the signals of MARVELS-1 b and c^*, the best-fit photometric amplitude is <0.2 mmag. We show the KELT data phased at these periods in Figure 5.

Lee et al. (2011) used these data to search for transits of the b component. They were able to rule out transits with a

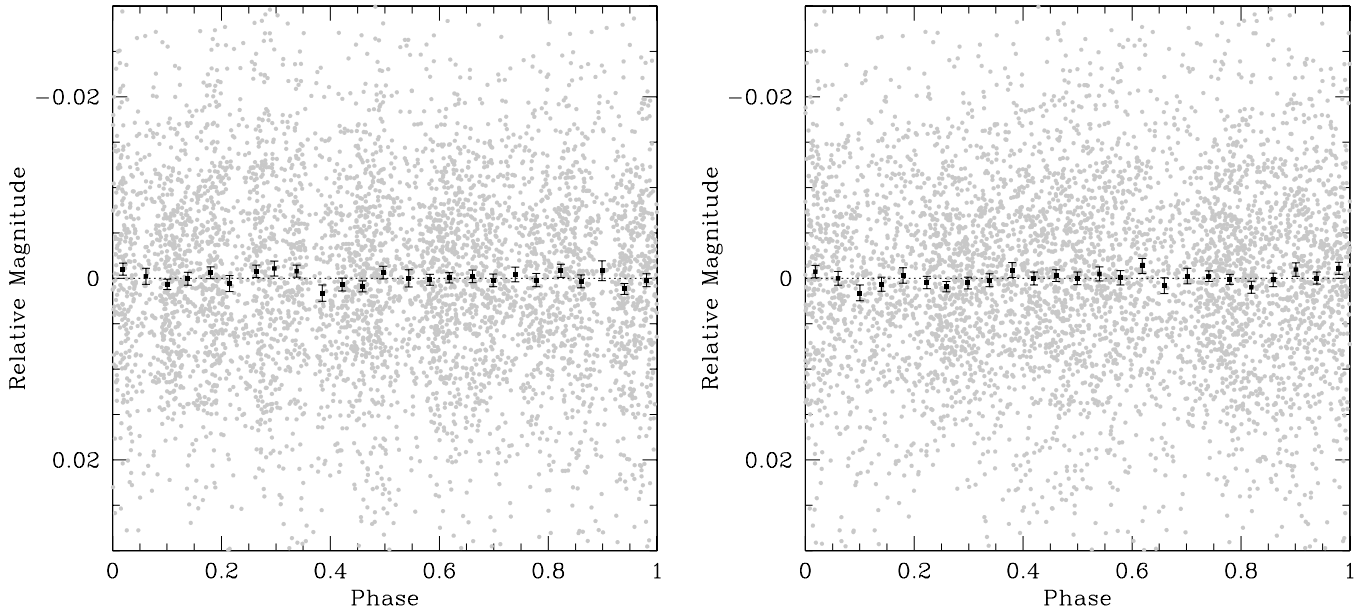

Figure 5. KELT photometry of MARVELS-1 phased at the periods of the *b* (left) and *c** (right) components. Gray points show the individual measurements and the black points show the data binned. The binned data show that the star is photometrically stable at the submillimagnitude level, with no evidence of either transits or stellar pulsations.

depth of ∼0.2% or greater, corresponding to companions of Jupiter radii or larger for the original estimate of the radius of the primary. If the *c** component exists, its a priori transit probability is ∼20%, and for our new stellar radius, a Jupiter radius companion at the period of the *c** component would produce a transit with a duration of ∼3 hr and a depth of ∼0.5%. For a strictly periodic transit, we can robustly exclude such a transit signal. However, we expect any transits of *c** to exhibit large transit timing variations (TTVs) with amplitudes of up to 10 hr due to dynamical interactions with *b* (see Section 5.3). Therefore, when phased to a single period, the transit will get smeared out, thereby lowering the S/N with which we detect or exclude the signal.

Nevertheless, we expect that such transits would probably still be detectable in the binned curves, even given the large possible TTVs: we can approximate the signal as being diluted by a factor of the duration/TTV amplitude, which is ∼(3 hr/10 hr)∗0.5% ∼ 0.15%, a level similar to that for which Lee et al. (2011) ruled out transits of the *b* component.

5. MCMC AND DYNAMICAL ANALYSIS

The novelty of this system demands a thorough analysis of the orbital parameters of the components and their dynamics. To this end, we explored the space of two-companion orbital fits to the RV data with a combination of MCMC analysis of the a posteriori Keplerian orbital elements and with a dynamical analysis of some of the families of solutions. This MCMC analysis was performed at a relatively early stage of the investigation, before the Keck data were available. As such it is based on HET data alone. The MCMC analysis was *not* renewed following the Keck data observations, since those data revealed that the *c** signal was likely spurious.

The period ambiguity from the aliasing of the period with the telescope observing constraints prevents our MCMC code from settling on a unique period for the *c** component, consistent with the heights of the sidelobes in Figure 3. We choose to focus on the 1.965 day period, which has the lowest residuals and is favored by the data. This inner period is consistent with a perfect 3:1 PC (the best-fit Keplerian solution has $|P_b/P_c - 3| \sim 10^{-4}$).

In summary, we find that most of the solutions in the MCMC chains are unstable on short timescales, but there do exist stable solutions. If the solutions we explore here describe an actual qualitative behavior of the system, then this system would exhibit significant perturbations, which would imply that the osculating Keplerian orbital elements would vary strongly and detectably on timescales of years, and that planetary transits might be intermittent as the inclinations of the companions oscillate. Were transits to occur, they might exhibit large (∼10 hr) timing variations.

5.1. MCMC Methodology

We analyzed the RV measurements using a Bayesian framework following Ford (2005) and Ford (2006a). We assume priors that are uniform in eccentricity, argument of pericenter, mean anomaly at epoch, velocity zero point, and logarithm of the orbital period. For the velocity amplitude (K) and jitter (σ_j), we adopted a prior of the form $p(x) = (x + x_o)^{-1}[\log(1 + x/x_o)]^{-1}$, with $K_o = \sigma_{j,o} = 1$ m s^{-1}, i.e., high values are penalized (for a discussion of priors, see Ford & Gregory 2007). The likelihood for RV terms assumes that each RV observation is independent and normally distributed about the true RV with a variance of $\sigma_i^2 + \sigma_j^2$, where σ_i is the published measurement uncertainty, and σ_j is a jitter parameter that accounts for additional scatter due to stellar variability, instrumental errors, and/or inaccuracies in the model (i.e., neglecting perturbations or additional, low amplitude planet signals).

We used an MCMC method based upon Keplerian orbit fitting to calculate a sample from the posterior distribution (Ford 2006b). We use the algorithm described in Ford (2005) to adaptively determine the appropriate step size to employ in our Markov Chains, initializing the algorithm with system parameters drawn from the best fits found using the frequentist approach described in Section 4. We calculated eight Markov Chains per MCMC realization, each with $\sim 2 \times 10^8$ states, and discarded the first half of the chains. We calculated Gelman–Rubin

Table 5
Orbital Elements at JD 2,455,200 (noon 2010 January 3 UT) for the Substellar Companions Resulting from the Keplerian MCMC Analysis of Section 5.2 in which Jitter Is Included as a Free Parameter

Quantity	Mean	$+1\sigma$	-1σ
P_b (days)	5.89537	0.00007	−0.00007
K_b (m s^{-1})	2572.4	4.3	−4.4
e_b	0.0158	0.0017	−0.0017
ω_b (°)	179.4	6.0	−6.1
M_b (°)	202.3	6.0	−6.0
$m_b \sin i_b$ ($M_{\rm Jup}$)	28.01	0.05	−0.05
P_c (days)	1.9649	0.0003	−0.0003
K_c (m s^{-1})	103.1	5.0	−4.7
e_c	0.101	0.056	−0.056
ω_c (°)	279.1	27.9	−40.1
M_c (°)	113.2	28.1	−29.6
$m_b \sin i_b$ ($M_{\rm Jup}$)	0.778	0.036	−0.034
log jitter	0.185	1.58	−2.41
χ^2	3.711	0.527	−0.52

Notes. Many of the solutions spanned by these parameters are dynamically unstable on short timescales. Note that the parameters of our best model for the system appear in Table 7, not here.

(Gelman & Rubin 1992) test statistics for each model parameter and several ancillary variables and found no indications of non-convergence among the individual chains (but see Section 5.2 for discussion of the differences between individual fits).

Following Keplerian fitting procedure, we attempted *n*-body DEMCMC fitting of the system (using the method described in ter Braak 2006; Payne & Ford 2011; Johnson et al. 2011), but found that either (1) the total number of observations is currently too small to constrain the parameter space sufficiently for this numerically intensive mechanism to converge in a reasonable time, or (2) no self-consist planetary fit is possible for this system.

To ensure that at least some fraction of the Keplerian fits are stable in the strongly-interacting regime expected of objects that are so close together and so massive, we took the results of the MCMC fits and injected those systems into the Mercury *n*-body package (Chambers 1999) and integrated them forward for $\sim 10^5$ yr ($\sim 10^7$ orbits). This exercise allowed us to distinguish the long-term stable fits to the data from those systems which happen to fit well but become unstable on very short timescales. We define "unstable" in a loose manner: we reject any systems which undergo a collision or change either of the planet's semi-major axes by >50%. This approach allowed significant variation in elements to occur but rejects systems which qualitatively change their architecture.

We assumed that all systems are coplanar and edge-on for the sake of this analysis, hence all of the masses used in our *n*-body analyses are *minimum* masses.

5.2. MCMC Results

We performed a number of independent MCMC simulations, all of which appeared to converge individually. However, the point of convergence often varied in different runs, which manifested itself in different sets of solutions having slightly different periods for the c^* component (i.e., the chains converged on local minima at the posterior probability distribution) essentially corresponding to the sidelobes for the inner period evident in Figure 3.

For the rest of this analysis we concentrate on those chains that converged on the local minimum characterized by the lowest values of the jitter ($\sim$5 m s^{-1}). These chains had an associated period for the c^* component of $P_c \sim 1.965$ days. The chains which converged to alternative local minima had significantly larger jitters ($\sim$10–50 m s^{-1}). The prior for jitter is intentionally chosen to have significant support even at realistically large jitters (which are highly unlikely due to the absence of strong stellar activity indicators in this star) so as to minimize the risk of overlooking interesting structure in the goodness-of-fit surface.

The results of our Keplerian MCMC fitting are presented in Figure 6 and summarized in Table 5. This analysis favors $P_c = 1.96493^{+0.00030}_{-0.00028}$ days and $P_b = 5.895374^{+0.000067}_{-0.000066}$ days, implying a period ratio that is consistent with exactly 3:1, within the uncertainties ($P_b/P_c = 3.00029721^{+0.00046}_{-0.00049}$). The MCMC fits constrain the outer object to have a low eccentricity $e_b = 0.016^{+0.002}_{-0.002}$, but allows a large spread in eccentricity for the c^* component, $e_c = 0.10^{+0.06}_{-0.06}$.

Table 6
Orbital Elements for the Substellar Companions Resulting from Integrations of the Long-term Stable Results Arising from the Keplerian MCMC Analysis of Section 5.2

Quantity	Mean Value at Epoch[a]	1 yr Mean[b]	1 yr Min[b]	1 yr Max[b]
P_b (days)	$5.89534^{+0.00006}_{-0.00005}$	5.944(1)	5.927(1)	5.961(1)
a_b (AU)	$0.0712776^{+0.0000005}_{-0.0000004}$	0.071332(8)	0.071200(10)	0.071468(9)
K_b (m s^{-1})	$2572.4^{+3.4}_{-3.2}$	...	...	...
e_b	$0.0168^{+0.0024}_{-0.0025}$	0.020(2)	0.016(2)	0.024(2)
ω_b(°)	$145.1^{+42.3}_{23.2}$	176.5(6.3)	162.8(8.4)	189.1(5.9)
P_c (days)	$1.9644^{+0.0002}_{-0.0002}$	1.943(2)	1.904(3)	1.981(4)
a_c (AU)	$0.034097^{+0.000003}_{-0.000002}$	0.033846(29)	0.033397(39)	0.034288(48)
K_c (m s^{-1})	$103.2^{+4.1}_{-4.4}$	...	...	...
e_c	$0.017^{+0.013}_{-0.014}$	0.058(7)	0.0006(3)	0.14(1)
ω_c(°)	$252.4^{+99.1}_{-192.8}$	143.0(36.5)	0.0(1)	360.0(1)

Notes. These elements span our favored dynamical solutions, however we cannot yet conclusively describe the true qualitative behavior of the system. In addition, the perturbations in these solutions make these Keplerian osculating elements an inadequate description of the system. See Table 4 for a note on error notation. Note that the parameters of our best model for the system appear in Table 7, not here.

[a] Results for JD−2,455,200, averaged over the 20 results from the MCMC fitting of Table 5 that were *also* long-term stable.

[b] Extracted from detailed 1 yr simulations initialized from the 20 individual starting conditions which underly the figures presented here in the "Mean Value at Epoch" column, with data output at *hourly* intervals and means, minimums, and maximums calculated.

5.3. Dynamical Analysis

As outlined in Section 5.1, the results of the Keplerian MCMC analysis in Section 5.2 were used as input to the Mercury *n*-body integrator (Chambers 1999) to integrate the systems for 10^5 yr. "Stepsize chaos" can be a source of error in numerical integrations, but it is negligible when the timestep Δt is smaller than the shortest physical timescale in the system by at least a factor of 10 or 20 (Rauch & Holman 1999). Each integration was carried out using a fixed timestep of $\Delta t = 0.01 P_c$, where P_c is the period of the inner planet. This exercise dramatically reduces the number of suitable orbital fits, as >99% of the solutions become unstable (using the approximate definition in Section 5.1) over the course of the 10^5 yr simulation.

The stable systems favor lower periods and eccentricities for the c^* component, as shown in the first column of Table 6 (we stress that the small number of systems ($\sim$20) that remained stable means that the values quoted suffer from small-number

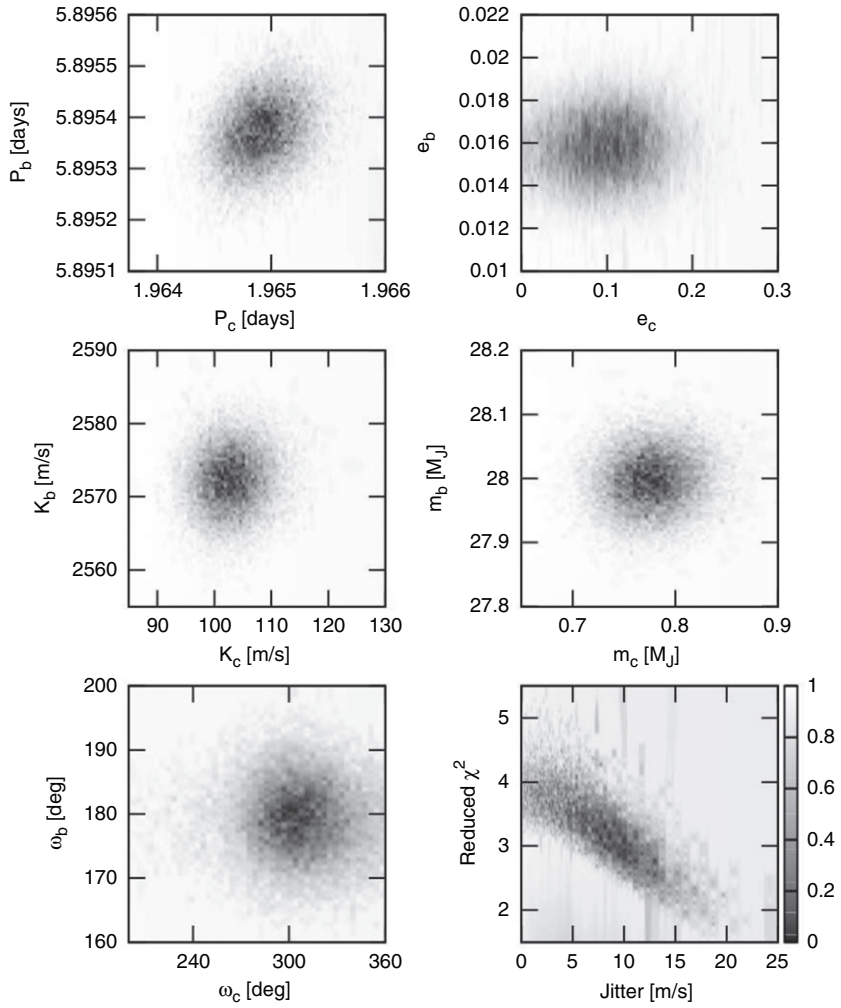

Figure 6. The results from the Keplerian MCMC fitting algorithm which converged to low jitter solutions. The top row contains (P_b, P_c) and (e_b, e_c), the second row (K_b, K_c) and (m_b, m_c), and the bottom row (ω_b, ω_c) and (jitter, χ^2). The shading indicates the distance from the mode. We find that the period of the b component is very tightly constrained to be $P_b = 5.895374^{+0.000066}_{-0.000067}$ days, while the c^* component is less tightly constrained, lying in the range $P_c = 1.96492^{+0.00029}_{-0.00028}$ days, where the uncertainties indicate $\sim 1\sigma$ confidence levels.

statistics). While the best-fit values for the period and eccentricity of the outer object are essentially unchanged, the best-fit values for the c^* component become $P_c = 1.9644^{+0.0002}_{-0.0002}$ days and $e_c = 0.017^{+0.013}_{-0.014}$, respectively. This means that the period ratio increases slightly to $\sim$3.001, but, more significantly, a much more circular orbit for the c^* component is strongly preferred (at least at the epoch of first observation—see below for further discussion).

The results of the long-term stability analyses enumerated in the first column of Table 6 should *not* be taken to be our final determination of the system parameters. The low fraction of the systems from the Keplerian fit which were stable indicates that while it is reassuring that there exist stable solutions within the neighborhood of the Keplerian fits, further work must be done to provide a reasonable statistical sample of such orbits. The orbits are *not* Keplerian over the duration of the fits (see below for further discussion), so a rigorous DEMCMC n-body fitting needs to be undertaken to generate such a sample of stable orbits (as outlined in Johnson et al. 2011). As noted in Section 5.1, our attempts at such an analysis were unsuccessful, as the routines did not converge. This could either be due to a lack of a sufficient number of high cadence observations, or may simply be due to it being impossible for a stable planetary system to give rise to the observed RV signal.

Figure 7 shows the detailed evolution over the course of 10^5 yr of various orbital elements in the system for one of the stable solutions. In addition to the period ratio, pericenters, semi-major axes, and apocenters, we also plot the resonant argument θ_1, θ_2, and θ_3 (Murray & Dermott 1999), defined as[19]

$$\begin{aligned} \theta_1 &= 3\lambda_b - \lambda_c - 2\omega_c \\ \theta_2 &= 3\lambda_b - \lambda_c - (\omega_c + \omega_b) \\ \theta_3 &= 3\lambda_b - \lambda_c - 2\omega_b. \end{aligned} \quad (1)$$

One can see that the system is in a resonant configuration, with θ_2 (gray asterisks) librating about 0° with an amplitude of $\sim$90°. One expects objects in resonance to have semi-major axes which oscillate slightly as a function of time (Murray & Dermott 1999), as demonstrated in the middle panel of Figure 7. Interestingly, in the case of MARVELS-1 this leads to period oscillations of $\sim$3% over the course of $\sim$200 days (<40 orbits of the outer body). Similarly, the eccentricity of the c^* component in this sample simulation changes between $\sim$0.01 and $\sim$0.1 in $\sim$100 days.

If this example simulation were typical of the real system, then such oscillations in period and eccentricity would be the

[19] Where λ is the usual mean longitude and we have taken the longitude of the ascending node $\Omega = 0$ for simplicity.

largest and fastest seen to date in any exoplanetary system. This result would have several implications.

1. For systems which interact strongly on short timescales, Laughlin & Chambers (2001) and Rivera & Lissauer (2001) demonstrated that Keplerian orbital fits are insufficient and that interaction terms need to be accounted for to fit the RV data. While this is patently the case here for MARVELS-1, in this situation the interactions are so strong and orbital perturbations occur on such short timescales that one can only report the range, manner, and timescale over which the quantity varies, in a manner similar to that undertaken for the proper orbital elements of asteroids (e.g., Knezevic et al. 2002).
2. The high masses and tight orbits of the bodies in TYC 1240 may provide an even more exquisite probe of a dynamically interacting system than the famed GJ 876 system (Marcy & Benitz 1989; Delfosse et al. 1998; Rivera et al. 2010): if a sufficient number of sufficiently precise RV observations can be taken with a sufficiently high cadence, then the dynamical interactions between the companions could reveal their inclinations and true masses. The advantage of the MARVELS-1 system is that nearly a full cycle of the orbital element variations takes place within a single observing season, significantly boosting observational plausibility.
3. Such strong interactions and associated large changes in orbital elements will likely drive significant TTVs in any hypothetical transit of the c^* component.
4. Our calculations were specifically for coplanar systems; however, if the companions are mutually inclined, then the precession of the orbit of the c^* component could be sufficiently strong and rapid that the system could quickly pass through episodes of transit and non-transit, further complicating any transit search.

We address point (1) in Table 6. We have taken all ∼20 stable systems from our long-term integrations and extracted the osculating elements at the epoch of the first observation. We report the mean and standard deviation of these parameters across the 20 solutions in the first data column. To capture how they vary with time, we have also calculated the mean and extremum values of these elements over the course of each of the 20 simulations and report the mean and standard deviation of these quantities across the 20 simulations in the other three data columns.

For instance, over the period of the n-body calculations of the stable solutions the eccentricity of the c^* component has a mean value of $e_c = 0.058$ and minimum and maximum values of $e_{c,\min} = 0.0006$, $e_{c,\max} = 0.14$, i.e., it changes from being almost perfectly circular to having an eccentricity of 0.14. The standard deviation figures are small, confirming that all 20 simulations display such oscillations.

We have conducted a preliminary investigation of the TTVs expected in such a system, assuming that the system is edge-on to the line of sight. We find that over the course of 1 yr of observations, TTVs of up to ±10 hr can occur. Such large variation would clearly be detectable, but would also have to be accurately accounted for in any initial search to ascertain whether the system transits at all (as any transit could easily be missed by many hours).

We conclude that there are some dynamically fascinating Newtonian (interacting) interpretations of the observed RV measurements, but that most solutions are unstable. This both adds to our suspicions that the two-companion model for the observed signal is incorrect and amplifies the extraordinary nature of the discovery if it is real.

6. POTENTIAL FALSE ALARMS

At this point in our analysis, we have an intriguing and exciting result: a clear, strong signal suggesting a super-planetary system in a near-perfect resonance with a strong likelihood of large and detectable dynamical effects, and the potential for transits.

But an application of a healthy skepticism reveals a few anomalies and coincidences that require consideration.

First, 3:1 resonances are rare (Wright et al. 2011). Second, such resonances are only perfect on average on long timescales; the actual orbital elements tend to librate about the equilibrium solution, so at any given epoch the period commensurability appears imperfect. These considerations make the apparent exactness of the commensurability suspicious. Third, the fact that the data admit but a few dynamically stable solutions (only 1% of our simulations are stable, and even those are highly dynamically active) suggests that we may not have settled on the correct solution.

Further, the relative phases of the planets are suspiciously coincidental, with both planets exhibiting RV extrema and zero-crossings simultaneously. To understand why this must be a coincidence, consider that for circular orbits these zero-crossings correspond to inferior and superior conjunction (i.e., transit and secondary eclipse for edge-on systems). As such, the zero-crossings of the b and c^* components should only appear simultaneous for a few special viewing angles.

Finally, it seems inherently unlikely that an unusual system such as this, for which there is no good analog among the thousands of stars previously surveyed for planets, would be the first system to emerge from a new planet survey (although, as we will see in Section 6.8, the selection criteria of MARVELS may make this not so unlikely as it seems).

All of these oddities could be explained if the RV signal were not actually the sum of two Keplerians, but some other shape that was approximately fit by such a sum. Could the faint, AO companions to MARVELS-1 have something to do with this unusual result?

Prudence requires both ruling out other explanations for the observed signal and understanding why MARVELS might be especially sensitive to such systems. In the face of the novelty of this system and the suspicions raised by the coincidences above, healthy skepticism demands that we rigorously consider all potential false positives to confirm that each has truly been ruled out.

6.1. Formal False Alarm Probability

The formal false alarm probability (FAP) for the planetary companion is virtually zero, due to its high amplitude compared to the rms residuals to the fit. We have confirmed this with a second-companion FAP calculation using bootstrapping (see Wright et al. 2009, for a thorough description). We subtracted the best-fit 6 day period Keplerian orbit from the velocities and assumed the null hypothesis, that the remaining scatter in the residuals was unpatterned noise of some character (possibly non-Gaussian). We then redrew these residuals (with replacement), added to them the original 6 day signal, and performed a thorough search of these artificial data for double-Keplerian solutions. We repeated this procedure to produce 1000

trial data sets. We recorded the rms value for the residuals for each trial and compared them with the residuals to the two-Keplerian fit of the authentic data set.

The sidelobes in the power spectrum of this data set make searching for the best two-companion solution difficult, since our L-M fitter (RVLIN) is easily trapped in local minima (i.e., sidelobes). We therefore thoroughly searched each bootstrapped dataset by testing the 10 most significant peaks in the residual periodogram, sufficient to find the best fit in the unscrambled data. Even with this extra effort, 0 trials in 1000 had an rms residual as low as the actual set, consistent with the amplitude of the true signal.

This result demonstrates that the 2 day signal is real in the sense that it is not a spurious periodogram peak introduced by the signal of the *b* component and unstructured noise interacting with the window function of the observations. Demonstrating that the signal is due to a planet and not some spurious *astrophysical, instrumental*, or *methodological* false positive requires eliminating alternative explanations (a task to which we devote the rest of this section) and verifying that the planet is physically plausible (i.e., that the derived orbit is dynamically stable, which we did in Section 5.3).

6.2. Stellar Pulsations

Practically speaking, any non-sinusoidal periodic RV signature measured at finite S/N can be well fit by a finite sum of sinusoids. It is therefore prudent to consider whether the entire 2.6 km s^{-1} signal is in fact due to stellar oscillations, and the signal from the apparent c^* component is in fact merely the most important harmonic component of a fundamental mode, or even a pulsational mode of the star excited by resonant interaction with the brown dwarf companion.

The lack of photometric variation (see Section 4) would seem to rule out any pulsation mechanism as the origin of the 2.6 km s^{-1} signal; nonetheless, we have investigated the expected photometric variation of many classes of variable stars and conclude that the most important false positive to consider for a star of this effective temperature and periods near 1–10 days is that of a low-amplitude Cepheid (of either type), such as Polaris.

Polaris is well studied (see, e.g., Bruntt et al. 2008, for a summary). Its pulsational RV signature is sinusoidal, and its amplitude has decreased from 6 km s^{-1} to about 0.5 km s^{-1} over the past century. Similarly, its photometric amplitude has decreased from around 140 mmag to as low as 30 mmag in *V* band in the year 2000, and as low as 10 mmag around 2005. Bruntt et al. (2008) find no evidence of overtones of the 4 day pulsation period in RVs or photometry. Usenko et al. (2005) find that the pulsational modes of Polaris are not obvious from the spectra in that the effective temperature of the star varies by no more than 100 K and does not correlate with pulsational phase (although Hatzes & Cochran 2000 find that the line bisector variations are detectable when the RV amplitude is 1.5 km s^{-1}).

A low-amplitude Cepheid is thus a particularly insidious false positive for a broad RV program, since it could in principle have a small (and easily overlooked) ∼10 mmag photometric variation, small line bisector variation, essentially no $T_{\rm eff}$ variation, and a large, easily detected ∼1 km s^{-1} RV signal reminiscent of a hot Jupiter companion.

There are several reasons this scenario, or a similar one, does not apply to MARVELS-1. The first is that most secondary pulsation modes are not harmonics of the dominant pulsation mode, but occur at a period with some non-integer period ratio (beat Cepheids usually have period ratios near 0.7 or 0.8, not 1/3). The second is that our prototype false positive, Polaris, shows no overtones at any period ratio, integer or otherwise. The third is that spectroscopic analysis of Lee et al. (2011) conclusively shows that MARVELS-1 is a dwarf, not a giant or supergiant, and so is not expected to have pulsational modes with periods near 6 days and in any case does not lie in the instability strip. Finally, our photometry in Section 4 places upper limits on the variability of MARVELS-1 that are nearly two orders of magnitude more stringent than the minimum variability of Polaris, our prototype confounder.

6.3. Stellar Activity and Star–Companion Interactions

While stellar activity can mimic the effects of planetary companions, it is an inadequate explanation in this case. MARVELS-1 does not show extraordinarily large Ca II H and K emission or large $v \sin i$ values, and so we do not expect variations of order 150 m s^{-1}, as seen here for the c^* component (Wright 2005), and certainly not at the level of the signal of MARVELS-1 *b*. The stability of the photometry precludes large spot-induced errors, and the low $v \sin i$ indicates that the observed signals are likely at much shorter periods than the rotation period of the star.

The 3:1 period commensurability is also inconsistent with one of the signals being due to stochastic stellar activity, which naïvely should not occur at a harmonic of the orbital period of MARVELS-1 *b*.

That said, the large mass and close separation of MARVELS-1 *b* suggest that we consider interactions between it and its host star as a possible source of unusual or novel effects on precise RV and bisector measurements. Depending on the true mass and temperature of MARVELS-1 *b*, it may detectably heat the host star's surface, altering its spectrum and convective flows there; it could cause a prolate distortion of the host star; or it could perhaps resonantly excite a normally dormant pulsation mode in the star at 1.965 days. Any of these effects could plausibly create a problematic RV signature with correlated bisector changes.

However, once again the photometric stability of MARVELS-1, documented in Section 4 at all of these frequencies, makes these possibilities very unlikely. Any variation in the output of MARVELS-1 of the sort described above strong enough to vary its spectral lines' positions by 100 m s^{-1} should also be apparent in the photometry, at least at the level of our photometric precision.

Further, it is difficult to construct any such scenario that produces significant power at three times the frequency of the *b* component, but not significant power at twice the period (which, for instance, prolate distortions would generate).

In short, any confounding effect along these lines would have to be previously undetected by RV surveys, generate large (100 m s^{-1}) RV variations at almost exactly three times the frequency of the *b* component (and at no other frequencies), and do so with no detectable photometric signature. We can think of no such effects.

6.4. Is MARVELS-1 b a Binary Brown Dwarf?

One source of false positive is that MARVELS-1 *b* is actually an equal mass binary brown dwarf with *total* minimum mass 28 $M_{\rm Jup}$, in a 3:2 orbit–orbit resonance. In this scenario, the variable quadropole moment of the binary brown dwarf would induce a small additional Doppler signature on MARVELS-1 at twice the frequency of the binary orbit, which we might observe as the 2 day signature. The binary would need to be nearly

equal mass, or else the fundamental orbital frequency would also produce a detectable signature.

Unfortunately, this particular false positive cannot be dispensed with quickly, since the parameters are rather well constrained and the predicted Doppler signature from such a scenario is similar to that seen in the observations. We present here a quick demonstration of this fact, using a toy model.

If we assume circular, unperturbed orbits for both the binary and the binary's orbit about MARVELS-1, denote the stellar mass M and the mass of each component of the binary $m(= 14\ M_{\rm Jup})$, denote the semimajor axis of the orbit of the center of mass of the binary around MARVELS-1 a (corresponding to period $P = 6$ days), and denote the total orbital separation $2d$ of the binary components from each other, we can use Kepler's laws to derive a rough, order-of-magnitude expression for the ratio d/a:

$$\left(\frac{d}{a}\right)^3 = \frac{1}{9}\frac{m}{M+2m}.$$

The semi-amplitude of the variation in the star's acceleration due to this variable quadropole for small d/a can be approximated as

$$\frac{K'}{K} = \frac{3}{2}\left(\frac{d}{a}\right)^2 \tag{2}$$

$$= \frac{3}{2}\left[\frac{1}{9}\frac{m}{M+2m}\right]^{\frac{2}{3}}, \tag{3}$$

where K' represents the semiamplitude of the perturbative signal. For $m/M \sim 4 \times 10^{-2}$ (assuming a high inclination for which the total BD binary mass is actually 80 Jupiter), we have $K'/K \sim 0.03$ or one part in 25. Our actual semiamplitude ratio from Section 3.4 is one part in 22, which is close enough that further analysis might be warranted.

Our healthy skepticism thus finds significant purchase here. In order to claim that the c^* component is a separate planet and not a spurious residual from the signal of a binary brown dwarf one must perform a more detailed analysis and show that such a scenario is dynamically impossible. We did not perform such an analysis for this system here, because we have a more important confounding effect to consider.

6.5. RV Signals from Fainter Stars

An obvious potential source of problems is the presence of the two companion stars described in Section 2.2.1, whose spectra might contaminate that of MARVELS-1 and produce complex and spurious velocity signatures.

We might also suspect that the entire RV signature is due to pulsations of one of the background objects, of the sort discussed in Section 6.2. This explanation also suffers from the fact that the photometry in Section 4 detects no variability for this system; if the pulsation modes are so dilute as to be invisible in our photometry, they should not appear as a 2.6 km s^{-1} signature in the RVs. This explanation also shares the difficulty that there are no classes of pulsing stars that exhibit the 3:1 period commensurability we see.

One general source of false positives with blended targets is a faint stellar binary whose signal is diluted by a brighter coincident star. In this case the Doppler signature of the binary is proportionally diluted, and the signal of the binary can be misinterpreted as a planetary signal (Torres et al. 2004b).

We can rule out the 0.″9 companion, which lies near the edge of our 2″ HRS fiber during nominal pointing. Seeing, tracking, and pointing variations should thus produce variable levels of contamination, and thus a variable Doppler signature that would lack any particular periodicity. Also, the contamination should be at a completely different level in our Keck velocities (since HIRES is slit-fed). Since we see a consistent signal in both the HET and Keck velocities, if the signal is due to a binary, then it must be the binarity of the 0.″15 object or another unresolved contaminant.

The 3:1 period commensurability further restricts the possibilities of a blend. If the source of the 100 m s^{-1} amplitude signal is to be attributed to the binary motion of one of the companion stars, we must accept the coincidence that the effect has a frequency surprisingly near a small integer multiple of the orbital frequency of MARVELS-1 b. Alternatively, if the entire RV signature of MARVELS-1 is to be due to a contaminating object, then we still must confront the novelty of this short-period 3:1 resonant system, except with significantly higher RV amplitudes (and thus masses and luminosities) for the objects (since their signal would be significantly diluted by MARVELS-1).

In short, it is difficult to construct a plausible scenario whereby two signals in a near-perfect 3:1 resonance are the product of anything other than Doppler signals from the primary star, MARVELS-1.

6.6. Effects of Spectral Contamination

In this section, we consider other sources of spurious Doppler signatures from spectral contamination. In the discussion below we will imagine how a cross-correlation procedure would be corrupted by the presence of a contaminating stellar spectrum. We will refer to a "template" spectrum (in practice, taken without the iodine cell in the beam) and an "epoch" spectrum (a subsequent observation, through the iodine cell). The change in velocity measured for an "epoch" spectrum with respect to the "template" spectrum is measured as the velocity shift at which the cross-correlation function (CCF) is maximized. This peak occurs at $\Delta v = v_e - v_t$, where v_e is the velocity of the star at epoch, and v_t was the velocity of the star during the template observation.

If a companion star with RV v_c were contaminating our spectra, then this contamination would produce a weak signal in the CCF at the velocity shift that aligns it with the template spectrum, $\Delta v = v_c - v_t$ (this effect is weak both because the spectral types do not match and because the contaminating spectrum is weak). There would also be a similar spurious peak from the contamination in the *template* spectrum correlating with the primary spectrum in the epoch observation, at $\Delta v = v_e - v_c$ (there is also a second-order peak from the contaminating spectrum interacting with itself at $\Delta v = 0$).

In this scenario, as the spectrum of MARVELS-1 shifts due to the influence of the brown dwarf, its spectrum will periodically align with the contaminating spectrum. When this happens, the "true" peak in the CCF at $\Delta v = v_e - v_t$ will align with the spurious peak at $v_c - v_t$. At values of v_e near v_c, the two CCF peaks will be blended, and the peak of their summed shape, which will be asymmetric, will not be at $v_e - v_t$, but will rather be "pulled" toward $v_c - v_t$ by an amount that depends on the amount of contamination and the magnitude of $v_c - v_t$.

Since the widths of these peaks are proportional to the line widths in the spectra, this effect will only be important for values of $|v_e - v_c|$ less than or similar to a typical line width, and the effect should decrease in magnitude rapidly for larger values.

The second spurious peak (at $\Delta v = v_e - v_c$) does not produce a similarly time-variable velocity anomaly; it will pull the true

CCF peak (at $\Delta v = v_e - v_t$) by a constant amount, which will be subtracted as a zero-point offset in the resulting differential velocities.

The time-variable component of this "peak pulling" could thus cause systematic errors in our measured velocities such that they are erroneously closer to the velocity of the contaminating star when the spectra are near alignment. This would manifest as an anomalous plateau near the preferred velocity, with a characteristic width determined by the typical line widths of the primary and contaminating lines. Since the amplitude of the RV variation from MARVELS-1 *b* is of similar magnitude to the line widths of MARVELS-1, we would expect all of the velocities to be affected to some degree (except at the preferred velocity where the spectra are perfectly aligned), but most severe when the velocity difference is greatest.

Although the AO companions to MARVELS-1 are too faint to contribute sufficient flux in the optical for this effect to be significant, we nonetheless explore it out of an abundance of caution. Below, we build a model for this effect and apply it to our Keck and HET velocities.

6.6.1. A General Model for "Peak Pulling"

We have modeled such an anomaly as $v_{\rm pert}$ where the velocities show a systematic tendency toward a preferred velocity v_0 when they are within a characteristic line width Δv of v_0:

$$v_{\rm pert} = k(e^{-((v-v_0)/\Delta v)^2})(v_0 - v),$$

where k is the magnitude of the effect.

We have generated artificial data assuming $\Delta v = 3.5$ km s^{-1}, $k = 0.25$, and $v_0 = 0$ as a perturbation on a sinusoidal signal of semiamplitude 3 km s^{-1}, and performed a sinusoidal best fit to the resulting velocities; the result is presented in Figure 8. Note the similarity of these curves to those in Figure 4.

Here, our healthy skepticism and abundant caution seem to have paid off. This "peak pulling" scenario naturally produces a residual signal to a sinusoidal fit whose dominant mode is at exactly three times the frequency of the primary signal.

This result can be understood from the symmetry produced by a pulling near the velocity zero, which produces a signal that shares the symmetries of a sinusoid, but in this case is slightly taller and narrower. As Figure 8 illustrates, the best-fit sinusoid and perturbed velocity curves meet at the $v = 0$ points (because $v_0 = 0$), and since the best fit will, by construction, follow the actual signal as closely as possible, it necessarily overestimates the true velocity near the $v = 0$ points and underestimates it near the crests. The best-fit curve thus crosses the true curve twice between the nodes, producing six points with zero residuals per full period, and so an apparent 3:1 period commensurability.

The actual perturbative signal does not have this characteristic: the residuals to the *true* RV curve have a different characteristic shape, as Figure 9 shows.

We have fit the HET data (as reduced with the HET template) under this scenario by assuming that the data can be modeled as a Keplerian plus a $v_{\rm pert}$ component with the free parameters given in the above equation. The best-fit solution is superior (rms = 14 m s^{-1}) to that given by a double-Keplerian to the HET data alone (rms = 19 m s^{-1}) and is consistent with the errors. In this solution we find $K = 3190$ m s^{-1}, significantly higher than the fit value for K in a single-Keplerian solution, and an orbit consistent with circular (best-fit $e = 0.0002^{+0.007}_{-0.0002}$). The best-fit perturbative parameters are $v_0 = -20$ m s^{-1}, $k = 0.30$, and $\Delta v = 4.1$ km s^{-1}, but are weakly constrained.

6.6.2. What Is the Source of Contamination?

There are three obvious candidates for the origin of a contaminating spectrum: the 0.″9 companion, the 0.″15 companion, and MARVELS-1 *b*. To first order, we expect none of these to be responsible: the AO companions are both 4 mag fainter than MARVELS-1 in the near-IR; if they are physically associated, they must be lower mass than MARVELS-1 (and so redder) and thus contribute negligibly to the spectrum in the optical iodine region. MARVELS-1 *b*, being substellar, should have no appreciable optical emission; indeed, any object bound to MARVELS-1 must have a comparable luminosity to the star itself to be a spectral contaminant. Nonetheless, our healthy skepticism requires that we carefully exclude each possibility.

The Keck velocities provide a powerful diagnostic, because, unlike with the fiber-fed HRS, the apparent velocity difference of MARVELS-1 and its contaminant will be a function of the position angle of slit during the measurement if the two objects have any measurable angular separation. Since the Keck 0.″861 slit was always rotated to the parallactic angle during our observations (Filippenko 1982), this would make the signal from the 0.″15 companion a strong function of hour angle of observation. Since MARVELS-1 was observed at hour angles ranging from +0.6 to −3.1, this effect would make the velocity perturbations appear essentially random, with no relationship to the phase of MARVELS-1 *b*. Further, if the 0.″9 companion were responsible, then its contribution would be highly variable, since its light would often miss the narrow HIRES slit entirely.

Interestingly, the Keck velocities fit the peak pulling model equally well (rms = 14 m s^{-1}), although with a high reduced χ^2 value due to the superior internal errors. The fact that the slit-fed HIRES sees a nearly identical signal to the fiber-fed HRS strongly suggests that the contaminating spectrum is located at small angular separation, indeed within 0.″15.

Although the Keck velocities show a similar signal, fitting the Keck and HET data jointly does not produce a good fit in this model (rms = 33 m s^{-1}), nor does fitting the HET data reduced with the Keck template alone (rms = 19 m s^{-1}). This illustrates that the form of the velocity perturbations from the contaminating spectrum is sensitive to the choice of template observation and the specific velocity reduction code used. This is perhaps not surprising, since the velocity perturbations are the result of a failure of the forward modeling process (which assumes uncontaminated spectra) and that different templates will have the contaminating spectrum Doppler shifted with respect to the primary spectrum by different amounts (at the time of the Keck template, $v = -2.0$ km s^{-1}; at the time of the HET template, $v = +1.3$ km s^{-1}).

Finally, we consider the possibility that the spectrum of MARVELS-1 *b* itself is a source of contamination, that is, that MARVELS-1 is a double-lined spectroscopic binary, and our spurious signal at 2 days is a result of incorrect modeling of the spectrum as being only single-lined. In this case, the RV amplitude of the secondary spectrum could be quite large, depending on the mass ratio of the system. If this spectrum is contributing to Doppler systematics, it might produce spurious (and small) peaks in the CCF at its velocity during the template observation, at zero velocity phase (i.e., during superior and inferior conjunction, when its spectrum aligns with that of MARVELS-1), and perhaps also at the velocity of any other contaminating spectrum (e.g., from one of the AO companions).

The fact that we achieve different qualities of fit using the Keck template and the HET template is consistent with this picture, since the velocity of the companion spectrum in the

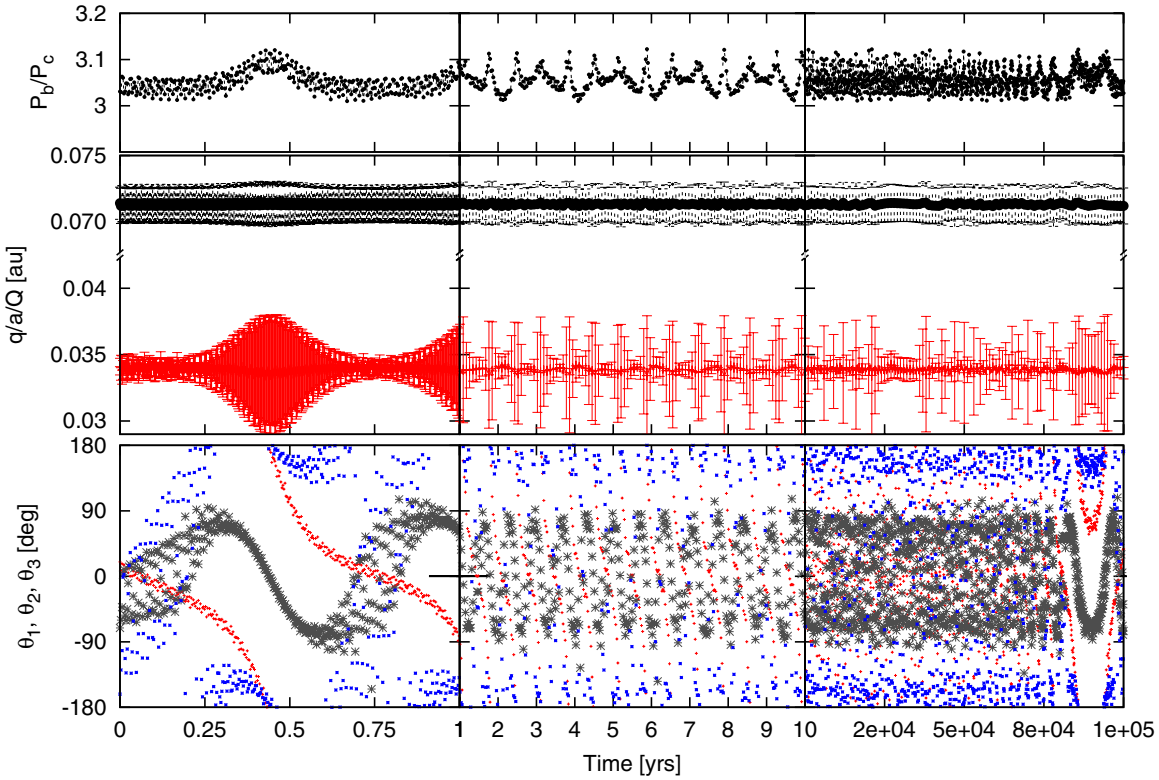

Figure 7. Orbital evolution for a sample long-term stable system. We select one of the long-term stable systems from our dynamical analysis and plot in detail the evolution of the orbital elements over 10^5 yr, plotting on the left-hand side the detailed evolution over a single year, in the center the stretch of data from 1 to 10 yr, and on the right the long-term evolution from 10 yr on to 10^5 yr. In the bottom panel we plot the three resonant arguments θ_1 (red), θ_2 (gray), and θ_3 (blue; see Equation (1) for definitions), showing that at least one of the arguments (θ_2, gray) is librating, albeit with a relatively large amplitude. In the second row we plot the range of orbital distances q (pericenter, bottom of bars), a (semimajor axis, central line), and Q (apocenter, top of bars) for the b and c^* components (black and red, respectively). The eccentricity of the more massive outer object changes very little, while the eccentricity of the c^* component oscillates from ∼0.01 to 0.1 over the course of ∼0.5 yr. Finally, the characteristic semi-major axis oscillations in a resonant system are present in this simulation (top row) and give rise to variations in the period ratio ∼3% on ∼0.5 yr timescales (top plot). If the c^* component is real, this result raises the exciting possibility of detecting such period and eccentricity oscillations directly from RV measurements.

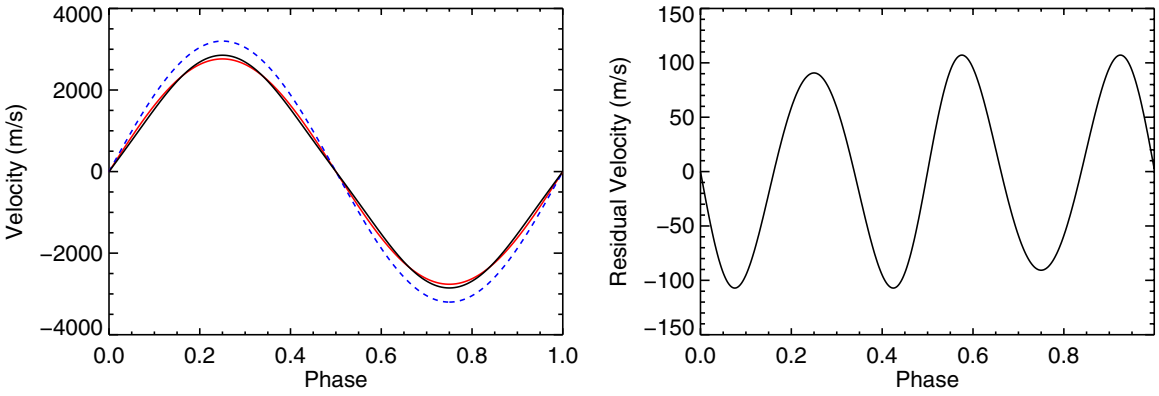

Figure 8. Left: velocities perturbed by a simple contamination model (black) and best circular fit (red). The blue dashed line illustrates the true, unperturbed velocity. Right: residual velocities (perturbed minus fit) showing the nearly sinusoidal, triple-peaked residuals (i.e., black curve minus red curve from the left panel). The shapes of these residuals are sensitive to the details of the contamination model, but will show a perfect 3:1 period commensurability for special values, like the ones we have chosen here. We phase both diagrams to have phase zero at the velocity zero with positive slope of the primary component. Compare these figures with Figure 4.

template observation should be different between the two telescopes due to its large intrinsic motion.

To check this possibility more rigorously, we constructed a peak-pulling model where the peak is pulled toward a variable velocity consistent with that expected from MARVELS-1 b, instead of a constant velocity v_0. We find that the χ^2 surface to fits to the HET data has a broad valley near its minimum, admitting significant motion of the secondary spectrum, proportional to Δv. Indeed, we find that we cannot constrain the implied mass ratio at all, with equally good fits existing at $(\Delta v, m_b/M) = (8.5\ \mathrm{km\ s^{-1}}, 0.65)$ and $(3.5\ \mathrm{km\ s^{-1}}, 20.8)$.

The former fit corresponds to a solution where MARVELS-1 b is stellar (that is, the system is a face-on binary, and the RV companion is not a brown-dwarf desert object at all). The latter fit seems rather unphysical, but corresponds to an essentially fixed contaminant (i.e., it is equivalent to our original peak-pulling motion with no motion of the contaminating spectrum). This corresponds to a scenario in which there is a fifth object

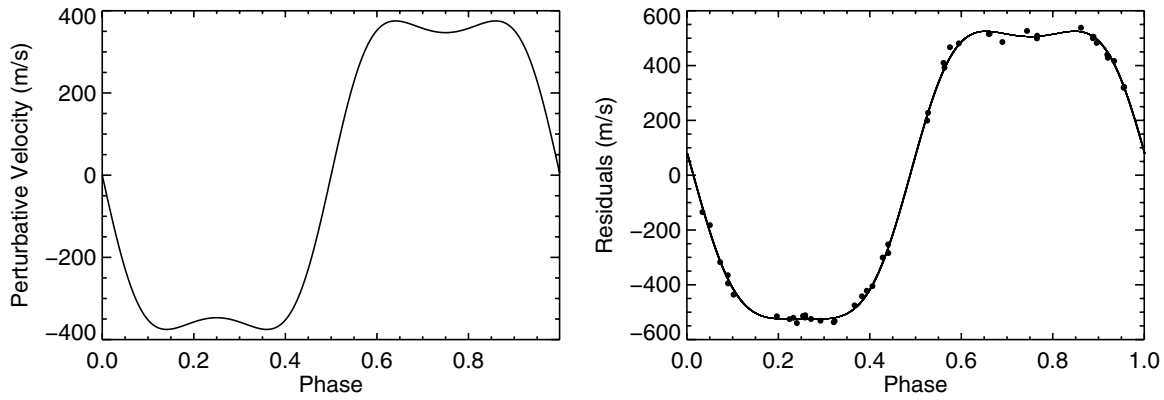

Figure 9. Left: the velocity perturbations $v_{\rm pert}$ to the *true* RV curve from the same model used in Figure 8 (i.e., blue curve minus black curve from the left side of Figure 8, as opposed to the *residuals* to the *fit* RV curve, which are shown in the right panel of Figure 8). Right: implied $v_{\rm pert}$ curve from best fit to HET RVs of a Keplerian-plus-"pulling" model. This model fits the HET data significantly better than the double-Keplerian model. We phase both diagrams to have phase zero at the velocity zero with positive slope of the primary component.

in the MARVELS-1, system, a chance alignment with a star of similar spectral type to MARVELS-1 but only 15%–30% of its flux, undetected in AO.

To confirm one of these or similar unlikely scenarios, we must identify intruding lines themselves in the spectrum and constrain whether they show significant Doppler motion. To break the degeneracy we find in the peak pulling models, this analysis must involve an actual measurement of the line widths and bisectors in the observed spectra.

6.6.3. Contamination Estimates and a Hunt for Contaminating Lines

We first performed a perfunctory examination of the 14 Keck spectra, which are of high S/N and resolution, to find any obvious signs of peak pulling. Such an analysis would not necessarily be dispositive, because the slit-fed HIRES line bisectors will be a strong function of the slit illumination profile, which may overwhelm any small line profile variations intrinsic to the source. Nonetheless, if the variations are sufficient to induce amplitudes of several hundred m s^{-1}, they may be visible.

We examined two regions in the red (outside of the iodine region): one region with strong telluric absorption and an adjacent order with several strong, deep stellar lines. We performed a simple cross-correlation in pixel space in the telluric region to account for night-to-night lateral shifts in the spectral format and interpolated the spectra onto a common scale. We then adopted an approximate wavelength solution for the CCD (obtained from a Th–Ar exposure on another night). Next, we applied the barycentric velocity shift to the wavelengths associated with each spectrum.

We selected three moderately deep and isolated stellar lines and fit Gaussians to their profiles, then inverted and normalized these profiles and interpolated them into velocity (log wavelength) space with zero velocity chosen to be the line center (as determined from the Gaussian fit). This approach allowed us to stack the line profiles for examination with improved S/N.

We show the stacked profiles for all 14 observations in Figure 10, with each component color-coded according to the measured RV of MARVELS-1. The line profile is clearly undergoing variations, most especially in the line wings at the velocity extremes. This result is consistent with an underlying contaminating line at each position with velocity at nearly exactly the average of the line profile positions and with a slightly larger line width than that of MARVELS-1. In the frame of the figure (the frame of MARVELS-1) a contaminating spectrum protrudes in the wings at the extreme velocities (emerging most clearly in the wings near ± 10 km s^{-1}).

6.6.4. CCF Bisector Analysis

Emboldened by the success of the peak pulling model at reproducing the observed RVs and its apparently successful prediction that there would be large line bisector variations, we proceed to perform a proper bisector analysis of the fiber-fed HRS data, which does not suffer from slit illumination issues. The aim of the bisector analysis was to measure the large line profile variations predicted by the peak pulling model and thereafter recreate the correlation between orbital phase and bisector change in an attempt to break the degeneracy between constant and variable velocity contaminants. In the context of planet-search surveys, there have been only a few instances where simulations of the bisector variation have been used to convincingly disentangle blended RVs (e.g., Santos et al. 2002). Conversely, the lack of a correlation between RV and bisector variations has sometimes been used to constrain the parameters of a system or to rule out blend scenarios (Torres et al. 2004a; Díaz et al. 2012).

Line profile bisectors have conventionally been used to distinguish between true RV signatures and spectral line asymmetries that mimic the existence of a companion (Toner & Gray 1988). However, long exposure times or the stacking of many individual exposures are required in high-resolution spectroscopy to achieve the S/N required for reliable line bisector analysis, which makes it difficult to measure short-term variations. Instead, we scrutinize the bisectors of CCFs constructed from the cross-correlation of observed spectra with numerical line masks (e.g., Baştürk et al. 2011). In addition to preserving line profile information, CCFs represent an "average" spectral line since they are based on multiple lines of different elements (Dall et al. 2006). Only changes to the ensemble of spectral line profiles are reflected in the shape of the CCF, making it less vulnerable to small-scale inconsistencies.

In an effort to study the true CCF profile, we used observations of MARVELS-1 on the HET HRS "red" CCD detector (6100–7600 Å), which is beyond the iodine region. The spectra consist of 25 echelle orders that were wavelength calibrated using the closest available Th–Ar hollow-cathode lamp calibration exposure taken during the night. Since the calibration exposures were neither simultaneous nor bracketed, the wavelengths calculated by this method may suffer from instrumental

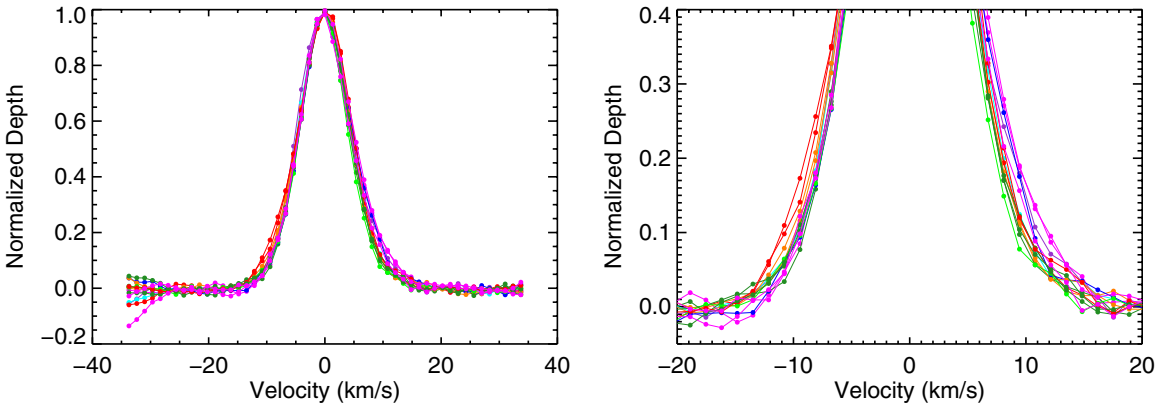

Figure 10. Left: stacked and normalized line profiles for 14 observations of MARVELS-1 from Keck. Colors indicate the measured radial velocity of MARVELS-1 (red indicating maximum redshift, etc.) Right: detail in the line wings, showing the effect of the underlying contaminating spectrum. When the star is most redshifted (in the barycentric frame of the MARVELS-1 system, indicated by the red lines) there is a clear excess in the blue (negative velocity) wing of the line, and conversely on the red wing of the most blueshifted lines.

shifts. However, since we are only using these spectra for CCF bisector analysis and not for precise RV extraction, this lack of high precision in the wavelength calibration will not effect our analysis. Only the five most well-behaved echelle orders were used, in an attempt to minimize arbitrary bisector variability. We also rejected five epochs due to low S/Ns, which produced faulty bisectors dominated by small-scale variation.

We computed the CCFs for each epoch by the cross-correlation of fully reduced and calibrated spectra with a weighted G_2 stellar template mask (Pepe et al. 2002; Baranne et al. 1996). The mask was created by us expressly for this purpose from an NSO FTS solar atlas (Kurucz et al. 1984). Consisting of 230 lines spanning the wavelength region between 6000 and 7800 Å, the mask has non-zero values coincident with the wavelengths of distinct unblended stellar lines and reflects the relative depth of absorption lines against the local continuum. For the cross-correlation, we use all lines that have a depth of 5% or more with respect to the stellar continuum, since we lose lines by setting the mask to zero in regions where the stellar signature is overwhelmed by telluric lines. The width of the mask lines is adjustable and set here to be 3 km s^{-1}, based on the resolution setting of the spectrograph.

Each spectral order was cross-correlated independently and the resulting CCFs added to attain a composite. The bisector was calculated as the loci of the midpoints of horizontal lines connecting the two wings of each composite CCF. Several measures have been used to quantify the shape of bisectors; we employ the bisector inverse slope (BIS), defined as the difference of average velocities between 10%–40% and 55%–85% of the total CCF depth (Queloz et al. 2001). The errors on the measurement of the BIS and the FWHM were determined from the dispersion in each value between different echelle orders. All of the measured BIS and FWHM values, along with their 1σ uncertainties, are presented in Table 8.

The bulk motion of a star would cause bisectors to oscillate around a mean bisector without changes in shape or orientation. However, the bisectors of MARVELS-1 change dramatically in the period observed, producing a large range in the BIS (Figure 11). We also show observations of σ Dra in the same wavelength region and calibrated by the same method for comparison; these bisectors are extremely stable and show hardly any change. The contrast between these stars emphasizes the fact that information about the system is encoded into the pattern of the MARVELS-1 bisectors.

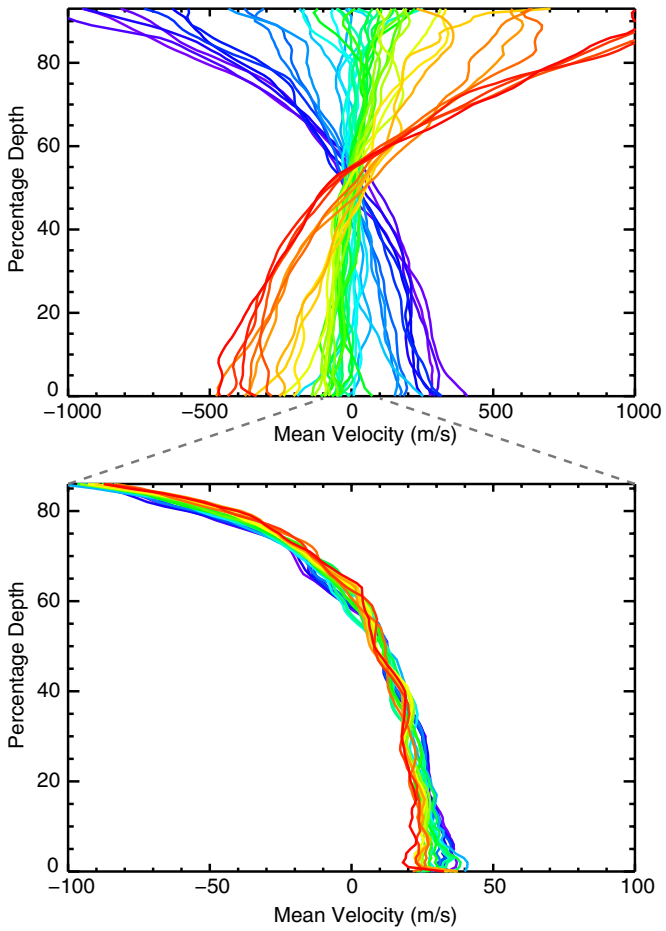

Figure 11. CCF bisectors, shifted by their CCF-measured radial velocities to align them for clarity. The colors are based on BIS values. Top: MARVELS-1. These bisectors change dramatically in both shape and orientation in the period observed. Bottom: σ Dra. Notice the factor of ten difference in the velocity axis range, demonstrating the stability of the σ Dra bisectors.

Figure 12 (left) shows a conspicuous relation between the BIS (measured from the CCF) and the cosine of the orbital phase angle, as calculated from the precise RV results (extracted by the iodine method). Specifically, the measured velocity and orbital phase are related as $v = k\cos(\phi)$, where k is a given velocity

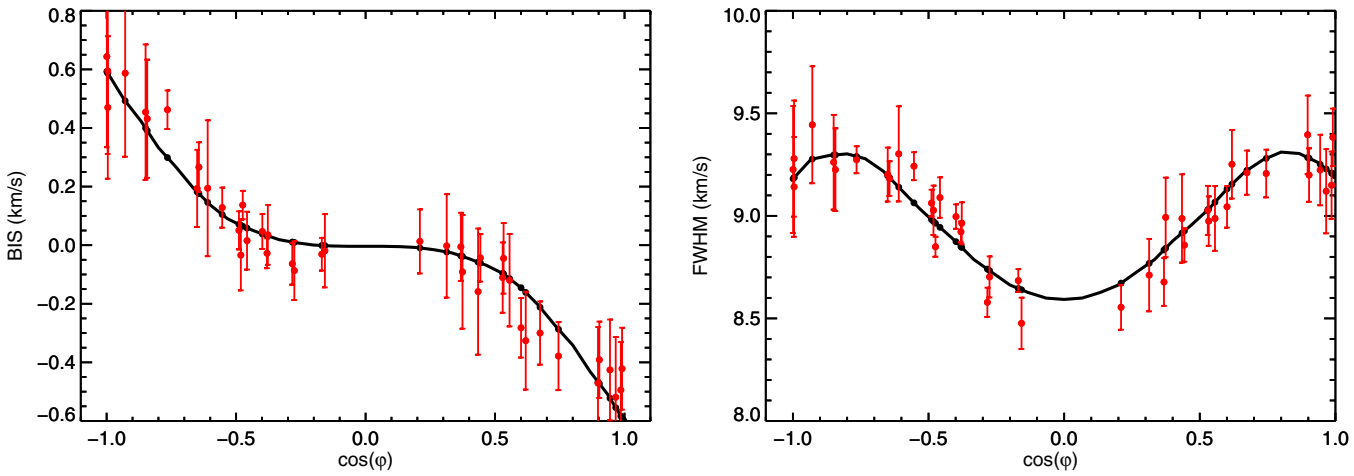

Figure 12. Left: points showing the relation between observed CCF bisector (BIS) values and the cosine of the measured phase angle (cosϕ) for MARVELS-1 (for convenience, the phase here is defined such that phase zero ($\varphi = 0$) occurs at the maximum radial velocity for the best-fit circular orbit). The solid line shows the BIS calculated from the simple model consisting of two shifting Gaussians, using parameters chosen to fit the observed BIS and FWHM values as a function of this orbital phase. Right: points as in left; line shows the FWHM calculated simultaneously from the two-Gaussian model. In both plots the bisector inverse spans and widths of the model and observed CCFs were measured in an identical fashion. The error bars are determined from the measurement variation between echelle orders.
(A color version of this figure is available in the online journal.)

semiamplitude. We choose to use the phase instead of directly using the RVs because the more precise iodine velocities are measured differently from the CCF method, where we simply measure the centroid of a fitted Gaussian. Even though the RVs produced by both methods are consistent within their respective uncertainties, we avoid any discrepancies by using a quantity that is agreed upon by both techniques.

The small values of BIS near $\cos(\phi) = 0$ and their symmetry about that value indicate that the primary and contaminating spectra are aligned at $v = 0$. Figure 12 (right) shows the FWHM values measured simultaneously with the BIS. This also has a minimum near $\cos(\phi) = 0$, reaffirming that the spectra are aligned at $v = 0$. This is consistent with the result from our peak pulling model that $v_0 \sim 0$.

6.6.5. A Two-component CCF Model

We attempted to reproduce this relation between BIS and $\cos(\phi)$ with a simple model. In keeping with the idea that spectral contamination from an unseen companion is leading to "peak pulling," we simulated a scenario where a large Gaussian (G_1, representing the true CCF of MARVELS-1 alone) shifts relative to a secondary Gaussian (G_2, representing the hypothesized contaminant) and periodically aligns with it at some velocity shift. At each phase step we calculated the BIS and FWHM of the combined CCF, produced by the sum of G_1 and G_2. A similar simulation with two Gaussians was performed by Santos et al. (2002) to recreate a linear BIS–RV relationship. They were able to detect a potential brown dwarf around a member of a binary system, using a constant velocity G_1 and four free parameters (including a variable G_2).

There are six free parameters in our model: the ratio of amplitudes of the two Gaussians (A_2/A_1), the FWHM of G_1 (w_1), the FWHM of G_2 (w_2), the mass ratio ($q = M_2/M_1$), the velocity semiamplitude of G_1 (K_1), and an adjustable offset between measured model BIS and observed BIS ($\Delta_{\rm BIS}$). This offset is included to allow for the fact that the observed CCF is not a perfect Gaussian, as assumed in the model. We explored the possibility of a constant velocity contaminant with this model and found that it was not possible to successfully match both BIS and FWHM with this configuration, although the BIS could be reproduced by itself. Thus, the behavior of the line profiles rules out the presence of a fifth object in chance alignment with this system.

A variable velocity contaminant renders an extremely viable model. In this scenario, the Gaussians undergo motion as in a binary system with a given mass ratio. In other words, the velocity semiamplitude of G_2 is determined by the mass ratio and the motion of G_1, or $K_2 = -qK_1$. Figure 12 (left) shows the result of our simulation, where both BIS and FWHM are matched *simultaneously* by mimicking a binary system. We arrive at our best-fit parameters using an AMOEBA routine (Nelder & Mead 1965) and conclude that the observations are modeled well by a binary system with $q = 1.20^{+0.02}_{-0.01}$, $K_1 = 3.05^{+0.01}_{-0.02}$ km s^{-1}, $A_2/A_1 = 18.93^{+0.83}_{-0.64}$%, $w_1 = 7.26^{+0.02}_{-0.03}$ km s^{-1}, $w_2 = 7.31^{+0.26}_{-0.26}$ km s^{-1}, and $\Delta_{\rm BIS} = -0.11 \pm 0.02$ km s^{-1}. Errors quoted here are formal errors on the parameters, which do not include systematic effects or covariances with the other parameters. Note that A_2/A_1 here is a proxy for the flux ratio of the binary. These formal uncertainties here were calculated by fixing all parameters, but one which was allowed to float, and determining the value of the floating parameter that increased χ^2 by 1 above its minimum value (30.5, with 34 degrees of freedom).

The fact that we are able to model the line profile variability so convincingly suggests that the culprit for the observed anomaly in the MARVELS-1 RV residuals is in fact a massive, relatively bright, bound companion.

6.6.6. Final Best Parameters for the MARVELS-1 Binary System

The mass ratio and amplitude of the RV primary component should be well represented by the q and K_1 parameters in our two-component CCF model. Interpretation of A_2/A_1 as the flux ratio of the two stars is complicated by that quantity's dependence on the choice of lines used in the two models; since we have not extracted the spectrum of the secondary here, we should anticipate that this is only a rough estimate of the true flux ratio.

The widths of the Gaussians (w_1, w_2) should correspond to the actual FWHM of the lines in the individual spectra (these

Table 7
Best Properties of the MARVELS-1 System

Property	Value	Source[a]
Per (d)	5.895322 ± 0.0002	PPM
T_0 (JD−2,440,000)	15509.039 ± 0.07	PPM
e	$0.0002\ ^{+0.007}_{-0.0002}$	PPM
ω (°)	130 ± 0.4	PPM
$K_{\rm Aa}$ (km s^{-1})	$3.05^{+0.01}_{-0.02}$	CCF
$K_{\rm Ab}$ (km s^{-1})	$3.66^{+0.06}_{-0.04}$	CCF
q	$1.20^{+0.02}_{-0.01}$	CCF
Flux ratio	∼0.2	CCF
FWHM (Aa) (km s^{-1})	$7.26^{+0.02}_{-0.03}$	CCF
FWHM (Ab) (km s^{-1})	7.31 ± 0.26	CCF
i (°)	2.47 ± 0.04	Section 6.6.6
$M_{\rm Aa}$ ($M_\odot$)	1.25 ± 0.06	Section 2.1
$M_{\rm Ab}$ ($M_\odot$)	1.04 ± 0.05	$M_{\rm Aa}/q$
rms (m s^{-1})	14.4	PPM
χ^2_ν	0.97	PPM

Note. [a] PPM: "peak pulling model" from Section 6.6.1. "CCF": BIS and FWHM analysis of HET spectra from Section 6.6.4.

values were computed after subtraction of the instrumental profile), and would indicate an equatorial rotational velocity $v \sin i = \mathrm{FWHM}/\sqrt{3} \sim 4$ km s^{-1} if we assume that a rotation broadening kernel of a uniform intensity disk with no differential rotation dominates the line width. We have validated this estimate by applying our CCF code to synthetic spectra and the solar spectrum convolved with rotational kernels or various equatorial velocities to calibrate our method. We find that the FWHM values we measure are consistent with $v \sin i$ values of 3.5–4.5 km s^{-1}, favoring the higher values.

The parameter $\Delta_{\rm BIS}$ encapsulates information about the inherent bisector span of the blended spectrum when the two spectra are perfectly aligned in velocity space. In any case, the formal uncertainty on these model parameters underestimates the true uncertainties in the physical parameters of the system because of the crudeness of our model of stellar spectral CCFs as pure Gaussians.

We calculate the inclination of the binary orbit from the binary mass function we infer from the CCF model:

$$\sin^3 i = \frac{K_1^3 q (1+q)^2 P}{2\pi G M_{\rm Aa}}, \quad (4)$$

where $M_{\rm Aa}$ is the mass of the primary star. Propagation of errors using the formal uncertainty on q and K and assuming $M_{\rm Aa} = 1.25 \pm 0.06\ M_\odot$ (Section 2.1) yields $i = 2.^\circ47 \pm 0.^\circ04$, where the uncertainty in i is dominated by the uncertainty in the mass of the primary.

We report our best system parameters in Table 7.

6.7. Summary of Potential False Alarm Consideration

We have found that the combination of the 3:1 period commensurability of the signals, their relative and absolute strengths, and the stability of the photometry rules out all scenarios that we have considered but three: a planetary companion in a 3:1 mean motion resonance, a binary brown dwarf in a 3:2 orbit–orbit resonance, and a 15%–30% spectral contaminant with a systemic velocity nearly identical to that of MARVELS-1 from an unresolved companion.

Table 8
Observed Values of BIS and FWHM for HET HRS Data of MARVELS-1

Time BJD−2,440,000 (UTC)	BIS (m s^{-1})	Uncertainty$_{\rm BIS}$ (m s^{-1})	FWHM (m s^{-1})	Uncertainty$_{\rm FWHM}$ (m s^{-1})
15177.6109	0.06	0.1	8.97	0.1
15178.5997	0.14	0.1	8.96	0.1
15180.7994	0.15	0.1	9.00	0.1
15181.7885	−0.01	0.1	9.03	0.1
15182.7878	−0.37	0.2	9.40	0.2
15183.5788	−0.06	0.2	8.99	0.2
15184.5782	0.12	0.1	9.09	0.1
15185.5711	0.75	0.3	9.23	0.3
15483.7415	−0.20	0.1	9.21	0.1
15483.7528	−0.22	0.2	9.25	0.2
15484.9464	0.08	0.1	8.48	0.1
15484.9577	0.07	0.1	8.68	0.1
15485.7397	0.53	0.2	9.23	0.2
15485.7510	0.56	0.2	9.26	0.2
15497.7059	0.69	0.3	9.44	0.3
15498.7192	0.57	0.1	9.27	0.1
15498.9215	0.30	0.2	9.30	0.2
15500.6947	−0.28	0.1	9.21	0.1
15500.9073	−0.32	0.2	9.22	0.2
15501.6961	−0.18	0.1	9.04	0.1
15507.6863	−0.02	0.2	8.99	0.2
15510.6632	0.30	0.1	9.20	0.1
15510.6715	0.37	0.1	9.18	0.1
15522.6391	0.15	0.1	9.06	0.1
15522.6469	0.07	0.1	9.03	0.1
15522.6547	0.24	0.0	8.85	0.0
15522.8492	0.04	0.1	8.58	0.1
15522.8570	0.02	0.1	8.70	0.1
15523.6459	0.06	0.1	8.86	0.1
15524.6390	−0.39	0.2	9.15	0.2
15527.6284	0.57	0.2	9.14	0.2
15576.7008	0.01	0.2	8.99	0.2
15577.7000	−0.32	0.1	9.38	0.1
15777.9371	−0.29	0.1	9.20	0.1
15779.9355	0.08	0.1	8.92	0.1
15782.9385	0.10	0.1	8.68	0.1
15783.9280	−0.42	0.2	9.12	0.2
15790.9292	0.10	0.2	8.71	0.2
15791.9106	0.23	0.1	9.24	0.1
15792.9209	0.70	0.3	9.28	0.3
15796.8955	0.12	0.1	8.55	0.1

Our line profile analysis definitively identifies MARVELS-1 *b* as the source of the contaminating spectrum, allowing us to dispose of the other hypotheses. The high inclination of this nearly face-on binary dilutes the true Doppler signature of the orbit down to values consistent with a brown-dwarf-desert candidate, and the effects of the contaminating spectrum create residuals to a sinusoidal fit that mimic a 3:1 resonance.

6.8. Similarities with Transit Searches

How can we understand why such a rare face-on binary system happens to be the first system detected by MARVELS? Fortunately, we can achieve this understanding without a thorough analysis of the MARVELS selection effects, which is far beyond the scope of this work.

MARVELS has observed a total of 3300 FGK stars with $V = 7.6$–12 (a magnitude limited selection) in 2008–2012 with each observed about 27 times over a 2 yr window. In contrast, other RV planet searches have typically searched of order 1000 stars. Because of its design, MARVELS necessarily targets stars

whose multiplicity, variability, and spectra properties are less well known beforehand. In addition, because the target stars are fainter, they are mostly likely to be blended with a significant contaminant (both because they are fainter and because they are more distant, and so there is a higher probability of a blended companion). MARVELS is thus especially sensitive to blend scenarios and binaries, relative to other RV planet searches, and needs to confirm its lowest amplitude detections in a manner similar to transit searches.

In a similar vein, the MARVELS program has also recently discovered the double-lined highly eccentric spectroscopic binary TYC-3010-1494-1, which masquerades as a modest-eccentricity brown dwarf candidate (Mack et al. 2013).

Nonetheless, the probability of the particular blend scenario of MARVELS-1 seems too low for such an object to be expected in the MARVELS survey. A rough order-of-magnitude calculation would estimate a ∼50% binary fraction for stars, that ∼10% of binaries are close binaries, that perhaps ∼10% have mass ratios such that the secondary would contaminate the spectrum, and that 0.01% of systems would be within 3 degrees of face-on (so the RV amplitude of the orbit is comparable to the line widths). This would suggest that MARVELS should encounter $3300 \times 0.5 \times 0.1 \times 0.1 \times 0.0001 \sim 0.02$ such systems. Either these estimates are collectively off by two orders of magnitude, or the MARVELS survey was quite unlucky to have encountered this system.

This situation is in some ways similar to that of transit searches, which have required extensive efforts to confirm and validate planet candidates, which must be sifted out from a large number of classes of false positive, in particular blends with eclipsing binary stars. For instance, Mandushev et al. (2005) found a similarly insidious form of false positive in the form of an eclipsing binary orbiting a slightly evolved F star that produced a nearly achromatic photometric signal indistinguishable from a transit in their photometric wide-field transit survey and produced a similar "peak pulling" signal to the one we see here.

7. NOMENCLATURE

Nomenclature standards for multiple systems are subjective and tricky to apply consistently. If we attempt to follow the Washington Multiplicity Catalog (WMC) standard as described in Raghavan et al. (2010) and recommended by the International Astronomical Union, then we must still decide how to organize these (possibly unbound) companions hierarchically and in what order to assign component letters.

The natural hierarchy here is unclear, because we might designate the 0.″9 companion "B" and group the other three components into a nearly unresolved "A" system, or we might put the 0.″15 and 0.″9 companions on equal footing and dub them "B" and "C" respectively. We choose the latter (consistent with our Figure 1). This makes the face-on short period binary MARVELS-1 Aa and MARVELS-1 Ab (where the lowercase letters follow the WMC convention for stars, but are conveniently consistent with the prior names for these objects, MARVELS-1 and MARVELS-1 *b*, respectively). We note that MARVELS-1 C is unlikely to be bound.

8. CONCLUSIONS

We have performed a thorough analysis of the complex MARVELS-1 system. Using AO imaging, we have identified a companion at 0.″9 separation that appears to be a foreground late M dwarf, and another at 0.″15 separation that appears to be a late K or early M dwarf associated with the primary, which we classify as an F9 dwarf.

The primary was previously thought to host a short-period companion occupying the "brown-dwarf desert," MARVELS-1 *b*, the first sub-stellar companion discovered with the MARVELS instrument. Follow-up RV measurements revealed strong deviations from a Keplerian solution, with amplitude ∼100 m s^{-1}and an orbital frequency exactly three times that of MARVELS-1 *b*.

We have identified three extraordinary explanations for the observed RV signature of MARVELS-1: a pair of substellar objects in a near-perfect 3:1 mean-motion resonance with strong dynamical interactions, a binary brown dwarf in a 3:2 resonance, and a blended stellar component contaminating the spectra, creating apparent residuals to a Keplerian solution at three times the observed period.

Identification of strong line bisector variations consistent with a contaminating spectrum confirms that the final scenario is the correct one, and our detection of significant RV motion of the contaminating spectrum confirms that it is due, in fact, to MARVELS-1 *b* itself, which is actually a stellar binary companion in a face-on orbit.

In this case, the concern raised over the unusual properties of the system caught an unlikely and insidious form of spectral contamination. A routine check for line profile variations would have caught the problem early, but there is little motivation for such a system at Keck, where large line profile variations are expected, even on RV stable stars, due to changes in the spectrograph and slit illumination. Bisector analysis is further hampered on unstabilized spectrographs by the lack of a precise wavelength scale outside the iodine region, and by the presence of iodine lines within the iodine region. Only in cases such as MARVELS-1 with large (3 km s^{-1}) RV variations, or with fiber-fed spectrographs, can bisector changes be obviously attributed to astrophysical, as opposed to instrumental, effects. Nonetheless, such cases may be common among hot Jupiters discovered with *Kepler*, and in such cases a line bisector analysis from Keck spectra will be an important validation step.

In the absence of such a check, the only indication that something was amiss was a "feeling" that the system was too unusual (the resonance was too perfect, the two-planet fit never good enough, the phases of the two "planets" too well matched) and the difficulty in identifying a good dynamical solution.

In summary, MARVELS-1 appears to be a stellar triple, with one presumably bound companion seen in AO and the other detected by RVs and line bisector variations. A foreground apparent companion is separated from this system by 0.″9 on the sky, bringing the total number of detected companions to the primary object to four.

We thank the referee, Dr. Alexandre Santerne, for a thorough and thoughtful review, and most especially his encouragement to more rigorously explore the possibility that MARVELS-1 is a face-on binary.

Funding for SDSS-III has been provided by the Alfred P. Sloan Foundation, the Participating Institutions, the National Science Foundation, and the U.S. Department of Energy. The SDSS-III Web site is http://www.sdss3.org/.

SDSS-III is managed by the Astrophysical Research Consortium for the Participating Institutions of the SDSS-III Collaboration including the University of Arizona, the Brazilian Participation Group, Brookhaven National Laboratory,

University of Cambridge, University of Florida, the French Participation Group, the German Participation Group, the Instituto de Astrofisica de Canarias, the Michigan State/Notre Dame/JINA Participation Group, Johns Hopkins University, Lawrence Berkeley National Laboratory, Max Planck Institute for Astrophysics, New Mexico State University, New York University, Ohio State University, Pennsylvania State University, University of Portsmouth, Princeton University, the Spanish Participation Group, University of Tokyo, University of Utah, Vanderbilt University, University of Virginia, University of Washington, and Yale University.

NSO/Kitt Peak FTS data used here were produced by NSF/NOAO.

The Center for Exoplanets and Habitable Worlds is supported by the Pennsylvania State University, the Eberly College of Science, and the Pennsylvania Space Grant Consortium.

This work was supported by the NASA Astrobiology Institute through the Penn State Astrobiology Research Center (grant NNA09DA76A).

We acknowledge the University of Florida High-Performance Computing Center for providing computational resources and support that have contributed to the results reported within this paper. This research has made use of NASA's Astrophysics Data System. This research has made use of the SIMBAD database, operated at CDS, Strasbourg, France.

The Hobby–Eberly Telescope (HET) is a joint project of the University of Texas at Austin, the Pennsylvania State University, Stanford University, Ludwig-Maximillians-Universität München, and Georg-August-Universität Göttingen. The HET is named in honor of its principal benefactors, William P. Hobby and Robert E. Eberly.

We thank the Penn State HET Science Director for the allocation of discretionary time necessary for this work, and the Penn State HET TAC for allocating regular time for the followup of MARVELS targets, including those described herein.

We thank NASA and NExScI for providing Keck time in the 2011B semester for the study of multiplanet systems (NExScI ID40/Keck ID N141Hr, PIs Wright and Ford). This work was supported by a NASA Keck PI Data Award, administered by the NASA Exoplanet Science Institute. Data presented herein were obtained at the W. M. Keck Observatory from telescope time allocated to the National Aeronautics and Space Administration through the agency's scientific partnership with the California Institute of Technology and the University of California. The Observatory was made possible by the generous financial support of the W. M. Keck Foundation. We thank the California Planet Survey consortium, and especially Andrew Howard and Geoff Marcy, for managing the queue, undertaking the Keck radial velocity measurements and template observation, and the precise Doppler analysis.

We thank Debra Fischer for use of her precise Doppler pipeline for the early stages of this effort, for encouraging a more thorough analysis of potential false positives, and for key insights into the pernicious nature of spectral contamination.

J.T.W. performed much of the analysis not mentioned below, oversaw and managed the overall research effort, and prepared this manuscript, including the incorporation of figures and text provided by the other authors. A.R., under the direction of J.T.W. and S.M., performed the CCF and line bisector analysis and provided the crucial proof that MARVELS-1 is a double-lined binary. J.T.W. and S.M. proposed for, obtained, and executed the HET observations and developed most of the false positive analysis. S.X.W. performed the raw reduction of the HET spectra and the precise Doppler analysis. M.J.P. performed the MCMC and DEMCMC dynamical analysis and stability tests and TTV calculations with guidance from E.B.F., who led the development of the MCMC, DEMCMC, and TTV algorithms used for the analysis. J.C. obtained the AO imaging, and he and Ji W. performed the image analysis and derived astrometry and photometry of the MARVELS-1 companions. B.S.G. and J.P. supplied the KELT photometry and provided its analysis. J.G. is PI of MARVELS and provided encouragement for and insight into the nature of the MARVELS-1 system and the MARVELS instrument. John W., B.L.L., P.A.C., J.I.G.H., L.G., L.D-F., G.F.P.M., M.A.G.M, L.N.C, R.L.C.O, and B.X.S. developed the stellar characterization pipeline and derived the new stellar parameters from high-resolution spectra based on a reanalysis of the FEROS spectra and new analysis of the APO spectra. John W. proposed for, observed, and reduced the APO spectra. Other authors provided significant contributions to this research through their membership in the SDSS consortium and/or the MARVELS team, and with useful comments on this paper.

E.B.F. and M.J.P. were supported by NASA Origins of Solar Systems Grant NNX09AB35G.

Work done by B.S.G. and J.E. was supported by NSF CAREER Grant AST-1056524.

J.P. and K.G.S. were supported by the Vanderbilt Office of the Provost through the Vanderbilt Initiative in Data-intensive Astrophysics (VIDA). The SME work at Vanderbilt was sponsored through the NSF Astronomy and Astrophysics Grant AST-1109612.

Funding for the Brazilian Participation Group has been provided by the Ministério de Ciência e Tecnologia (MCT), Fundação Carlos Chagas Filho de Amparo à Pesquisa do Estado do Rio de Janeiro (FAPERJ), Conselho Nacional de Desenvolvimento Científico e Tecnológico (CNPq), and Financiadora de Estudos e Projetos (FINEP).

G.F.P.M. acknowledges financial support by CNPq (476909/2006-6 and 474972/2009-7) and FAPERJ (APQ1/26/170.687/2004) grants.

L.G. acknowledges financial support provided by the PAPDRJ CAPES/FAPERJ Fellowship. L.D.F. acknowledges a PhD scholarship from CAPES/Brazil.

Facility: Keck:I

REFERENCES

Baranne, A., Queloz, D., Mayor, M., et al. 1996, A&AS, 119, 373
Baştürk, Ö., Dall, T. H., Collet, R., Lo Curto, G., & Selam, S. O. 2011, A&A, 535, A17
Borucki, W. J., Agol, E., Fressin, F., et al. 2013, Sci, 340, 587
Bruntt, H., Evans, N. R., Stello, D., et al. 2008, ApJ, 683, 433
Butler, R. P., Marcy, G. W., Williams, E., et al. 1996, PASP, 108, 500
Chambers, J. E. 1999, MNRAS, 304, 793
Collier Cameron, A., Wilson, D. M., West, R. G., et al. 2007, MNRAS, 380, 1230
Dall, T. H., Santos, N. C., Arentoft, T., Bedding, T. R., & Kjeldsen, H. 2006, A&A, 454, 341
Delfosse, X., Forveille, T., Mayor, M., et al. 1998, A&A, 338, L67
Delfosse, X., Forveille, T., Ségransan, D., et al. 2000, A&A, 364, 217
Díaz, R. F., Santerne, A., Sahlmann, J., et al. 2012, A&A, 538, A113
Diolaiti, E., Bendinelli, O., Bonaccini, D., et al. 2000, in ASP Conf. Ser. 216, Astronomical Data Analysis Software and Systems IX, ed. N. Manset, C. Veillet, & D. Crabtree (San Francisco, CA: ASP), 623
Eisenstein, D. J., Weinberg, D. H., Agol, E., et al. 2011, AJ, 142, 72
Filippenko, A. V. 1982, PASP, 94, 715
Ford, E. B. 2005, AJ, 129, 1706
Ford, E. B. 2006a, ApJ, 642, 505

Ford, E. B. 2006b, in ASP Conf. Ser. 352, New Horizons in Astronomy: Frank N. Bash Symposium, ed. S. J. Kannappan, S. Redfield, J. E. Kessler-Silacci, M. Landriau, & N. Drory (San Francisco, CA: ASP), 15
Ford, E. B., & Gregory, P. C. 2007, in ASP Conf. Ser. 371, Statistical Challenges in Modern Astronomy IV, ed. G. J. Babu & E. D. Feigelson (San Francisco, CA: ASP), 189
Ge, J., Mahadevan, S., Lee, B., et al. 2008, in ASP Conf. Ser. 398, Extreme Solar Systems, ed. D. Fischer, F. A. Rasio, S. E. Thorsett, & A. Wolszczan (San Francisco, CA: ASP), 449
Gelman, A., & Rubin, D. B. 1992, StaSc, 7, 457
Ghez, A. M., Salim, S., Weinberg, N. N., et al. 2008, ApJ, 689, 1044
Gunn, J. E., Siegmund, W. A., Mannery, E. J., et al. 2006, AJ, 131, 2332
Hatzes, A. P., & Cochran, W. D. 2000, AJ, 120, 979
Howard, A. W., Johnson, J. A., Marcy, G. W., et al. 2009, ApJ, 696, 75
Howard, A. W., Johnson, J. A., Marcy, G. W., et al. 2010, ApJ, 721, 1467
Howard, A. W., Johnson, J. A., Marcy, G. W., et al. 2011a, ApJ, 726, 73
Howard, A. W., Johnson, J. A., Marcy, G. W., et al. 2011b, ApJ, 730, 10
Johnson, J. A., Howard, A. W., Marcy, G. W., et al. 2010, PASP, 122, 149
Johnson, J. A., Payne, M., Howard, A. W., et al. 2011, AJ, 141, 16
Knezevic, Z., Lemaître, A., & Milani, A. 2002, in Asteroids III, ed. W. F. Bottke, Jr., A. Cellino, P. Paolicchi, & R. P. Binzel (Tucson, AZ: Univ. Arizona Press), 603
Konacki, M., Torres, G., Sasselov, D. D., & Jha, S. 2003, ApJ, 597, 1076
Kraus, A. L., & Hillenbrand, L. A. 2007, AJ, 134, 2340
Kurucz, R. L., Furenlid, I., Brault, J., & Testerman, L. 1984, Solar Flux Atlas from 296 to 1300 nm (Sunspot, NM: National Solar Observatory)
Laughlin, G., & Chambers, J. E. 2001, ApJL, 551, L109
Lee, B. L., Ge, J., Fleming, S. W., et al. 2011, ApJ, 728, 32
Mack, C. E., III, Ge, J., Deshpande, R., et al. 2013, AJ, 145, 139
Mandushev, G., Torres, G., Latham, D. W., et al. 2005, ApJ, 621, 1061
Marcy, G. W., & Benitz, K. J. 1989, ApJ, 344, 441
Murray, C. D., & Dermott, S. F. 1999, Solar System Dynamics (Cambridge: Cambridge Univ. Press)
Nelder, J. A., & Mead, R. 1965, CompJ, 7, 308
O'Donovan, F. T., Charbonneau, D., Alonso, R., et al. 2007, ApJ, 662, 658
Payne, M. J., & Ford, E. B. 2011, ApJ, 729, 98
Pepe, F., Mayor, M., Galland, F., et al. 2002, A&A, 388, 632
Pepper, J., Pogge, R. W., DePoy, D. L., et al. 2007, PASP, 119, 923
Piskunov, N. E., & Valenti, J. A. 2002, A&A, 385, 1095
Queloz, D., Henry, G. W., Sivan, J. P., et al. 2001, A&A, 379, 279
Raghavan, D., McAlister, H. A., Henry, T. J., et al. 2010, ApJS, 190, 1
Ramsey, L. W., Adams, M. T., Barnes, T. G., et al. 1998, Proc. SPIE, 3352, 34
Rauch, K. P., & Holman, M. 1999, AJ, 117, 1087
Rivera, E. J., Laughlin, G., Butler, R. P., et al. 2010, ApJ, 719, 890
Rivera, E. J., & Lissauer, J. J. 2001, ApJ, 558, 392
Santerne, A., Díaz, R. F., Moutou, C., et al. 2012, A&A, 545, A76
Santos, N. C., Mayor, M., Naef, D., et al. 2002, A&A, 392, 215
Shetrone, M., Cornell, M. E., Fowler, J. R., et al. 2007, PASP, 119, 556
Siverd, R. J., Pepper, J., Stanek, K., et al. 2009, in IAU Symp. 253, Transiting Planets, ed. F. Pont, D. Sasselov, & M. J. Holman (Cambridge: Cambridge Univ. Press), 350
Tabernero, H. M., Montes, D., & González Hernández, J. I. 2012, A&A, 547, A13
ter Braak, C. J. F. 2006, Stat. Comput., 16, 239
Toner, C. G., & Gray, D. F. 1988, ApJ, 334, 1008
Torres, G., Andersen, J., & Giménez, A. 2010, A&ARv, 18, 67
Torres, G., Konacki, M., Sasselov, D. D., & Jha, S. 2004a, ApJ, 609, 1071
Torres, G., Konacki, M., Sasselov, D. D., & Jha, S. 2004b, ApJ, 614, 979
Tull, R. G. 1998, Proc. SPIE, 3355, 387
Usenko, I. A., Miroshnichenko, A. S., Klochkova, V. G., & Yushkin, M. V. 2005, MNRAS, 362, 1219
Valenti, J. A., & Piskunov, N. 1996, A&AS, 118, 595
Wang, S. X., Wright, J. T., Cochran, W., et al. 2012, ApJ, 761, 46
Wang, X., & Wright, J. T. 2011, BAAS, 217, 253.08
Wisniewski, J. P., Ge, J., Crepp, J. R., et al. 2012, AJ, 143, 107
Wizinowich, P., Acton, D. S., Shelton, C., et al. 2000, PASP, 112, 315
Wright, J. T. 2005, PASP, 117, 657
Wright, J. T., & Howard, A. W. 2009, ApJS, 182, 205
Wright, J. T., Upadhyay, S., Marcy, G. W., et al. 2009, ApJ, 693, 1084
Wright, J. T., Veras, D., Ford, E. B., et al. 2011, ApJ, 730, 93